

Colistin-Functionalized Nanoparticles for the Rapid Capture of *Acinetobacter baumannii*

By

Sinead Emily Miller

Thesis

Submitted to the Faculty of the
Graduate School of Vanderbilt University
in partial fulfillment of the requirements
for the degree of

MASTER OF SCIENCE

in

Biomedical Engineering

December, 2015

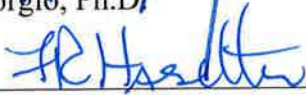
Nashville, Tennessee

Approved:

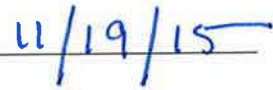
Date:



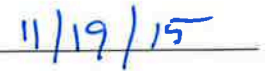
Todd D. Giorgio, Ph.D.



Frederick R. Haselton, Ph.D.



11/19/15



11/19/15

ACKNOWLEDGEMENTS

First, praise and thanks goes to the Lord Jesus Christ for blessing me with the ability to perform this work. I sincerely thank my advisor, Dr. Todd D. Giorgio, for giving me the opportunity to join his lab at Vanderbilt University. Without his persistent support and guidance this thesis would not have been possible. I thank Charleson S. Bell and Raquel Mejias for their academic support, friendship, and feedback on my work. All Giorgio lab members, past and present, have been very encouraging and I am grateful for that. Also, I want to express my love and gratitude to my family and friends. Finally, I want to thank the Department of Defense (DoD) (W81XWH-13-1-0397) for providing financial support for this work.

TABLE OF CONTENTS

	Page
ACKNOWLEDGEMENTS	iii
LIST OF TABLES	vi
LIST OF FIGURES	vii
Chapter	
1. Introduction	1
1.1. <i>Clinical need for reduction of A. baumannii transmission</i>	1
1.2. <i>A. baumannii presence in water supplies</i>	2
1.3. <i>Methods used to reduce microorganism contamination of water supplies</i>	2
1.3.1. <i>Nanofiltration membranes</i>	4
1.3.2. <i>Nanoporous ceramic</i>	6
1.3.3. <i>Nanofibers</i>	7
1.3.4. <i>Nanocatalysts</i>	8
1.3.5. <i>Magnetic nanoparticles</i>	9
1.4. <i>Aims addressed in this thesis project</i>	11
1.4.1. <i>Synthesize and physically characterize colistin-functionalized gold nanoparticles (Col-PEG-AuNPs)</i>	11
1.4.2. <i>Evaluate and characterize Col-PEG-AuNP binding with A. baumannii</i>	12
1.5. <i>Organization of Thesis</i>	12
2. Materials and Methods	14
2.1. <i>Materials</i>	14
2.2. <i>Methods</i>	14
2.2.1. <i>Synthesis of Col-PEG-AuNPs</i>	14
2.2.2. <i>Synthesis of polyethylene glycol-functionalized gold nanoparticles (PEG- AuNPs)</i>	15
2.2.3. <i>Physical characterization of Col-PEG-AuNPs and PEG-AuNPs</i>	15
2.2.4. <i>Confirmation of Colistin-PEG₃₄₀₀-OPSS and NHS-PEG₃₄₀₀-OPSS conjugation to AuNPs</i>	16
2.2.5. <i>Cell culture</i>	17
2.2.6. <i>In vitro cytotoxicity studies</i>	17
2.2.7. <i>In vitro hemocompatibility</i>	18
2.2.8. <i>A. baumannii binding</i>	18
2.2.9. <i>AuNP standard concentration curve</i>	19
2.2.10. <i>A. baumannii binding kinetics</i>	19
2.2.11. <i>Statistical analysis</i>	20

2.2.12. <i>Ethical compliance</i>	20
3. Results	21
3.1. <i>Preparation of Col-PEG-AuNPs and PEG-AuNPs</i>	21
3.2. <i>Characterization of functionalized AuNPs</i>	23
3.3. <i>Confirmation of Colistin-PEG₃₄₀₀-OPSS and NHS-PEG₃₄₀₀-OPSS conjugation to AuNPs</i>	23
3.4. <i>In vitro cytotoxicity studies</i>	29
3.5. <i>In vitro hemocompatibility</i>	31
3.6. <i>Nanoparticle binding to A. baumannii</i>	32
3.7. <i>A. baumannii binding kinetics</i>	36
4. Summary	38
Appendix	40
REFERENCES	47

LIST OF TABLES

Table	Page
1. NP zeta potentials	24
2. NP size distributions	25
3. Percent hemolysis caused by Col-PEG-AuNPs and PEG-AuNPs.....	41
4. Percent hemolysis caused by free colistin.....	42

LIST OF FIGURES

Figure	Page
1. TEM image of <i>A. baumannii</i>	1
2. SEM images of CNTs (Source [26]).....	5
3. SEM images of cellulose nanofibers (Source [41]).....	8
4. Col-PEG-AuNP synthesis scheme and proposed interaction with <i>A. baumannii</i>	22
5. TEM images of AuNPs, PEG-AuNPs, and Col-PEG-AuNPs.....	23
6. DLS size estimates of AuNP, PEG-AuNP, and Col-PEG-AuNP.....	25
7. H ¹ NMR spectrums supporting Col-PEG ₃₄₀₀ -OPSS conjugation to AuNPs.....	27-28
8. Cellular compatibility of Col-PEG-AuNPs and PEG-AuNPs.....	30
9. Cellular compatibility of free colistin.....	31
10. STEM images confirming Col-PEG-AuNP association with <i>A. baumannii</i>	34-35
11. Binding kinetics of Col-PEG-AuNP association with <i>A. baumannii</i>	37
12. TEM-EDS of Col-PEG-AuNPs.....	40
13. EDS spectrum confirming Col-PEG-AuNP association with <i>A. baumannii</i>	43
14. Elemental composition of <i>A. baumannii</i>	44
15. EDS spectrum confirming that PEG-AuNPs do not associate with <i>A. baumannii</i>	45
16. AuNP standard concentration curve.....	46

CHAPTER 1

Introduction

1.1. Clinical need for reduction of A. baumannii transmission

Acinetobacter baumannii, a Gram-negative coccobacillus with a multi-drug resistant (MDR) phenotype, is commonly found in soil, water, mucous membranes, vegetables, and on human skin [1]. Individuals with a compromised immune system, diabetes, or wounds can suffer from life-threatening infections resultant from *A. baumannii*. These infections can lead to widespread inflammation, blood clotting, multiple organ failure, pneumonia, septic shock, and death [1]. *A. baumannii* is responsible for 2% to 10% of Gram-negative bacterial infections worldwide and has an associated mortality rate reaching up to 70% [2]–[4].

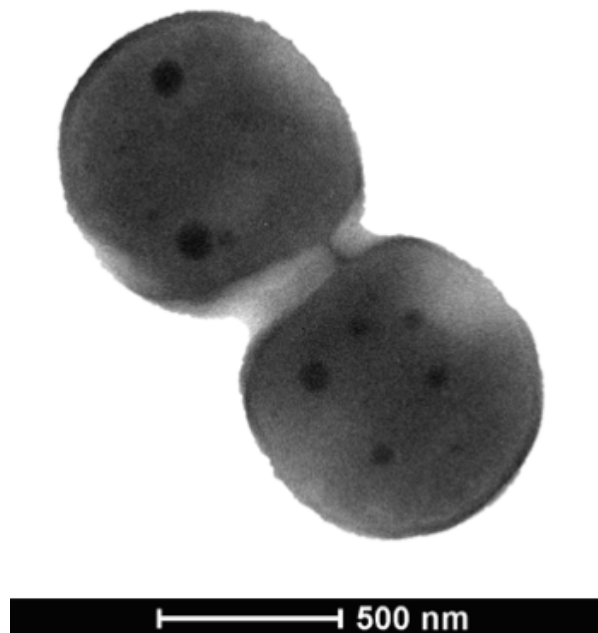


Figure 1.1. Transmission electron microscopy (TEM) image of *A. baumannii*.

1.2. A. baumannii presence in water supplies

The spread of *A. baumannii* occurs via human contact and through contact with contaminated food, soil, water, or hospital equipment [5]. *A. baumannii* has been detected in freshwater ecosystems, sewage, wastewater, drinking water, and groundwater supplies [5], [6]. Infections resultant from *A. baumannii* and other Gram-negative bacteria can be transmitted by contaminated drinking water [7]. Freshwater and marine water ecosystems are natural sources of *Acinetobacter* species and can also serve as effective means of *Acinetobacter* transmission. Mortality rates attributed to *A. baumannii* nosocomial infections are 20-70%, which is higher than most other bacterial species. Therefore, steps must be taken to prevent the transmission of infections caused by *A. baumannii*. Elimination of *A. baumannii* from water is one important step that can be taken to reduce the transmission of this bacterium.

1.3. Methods used to reduce microorganism contamination of water supplies

It is well documented that many public health and environmental problems are resultant from contamination of water with microorganisms, including *A. baumannii* [8],[9]. In 2014, it was reported by the World Health Organization that over 1.8 billion people use a contaminated water supply, with the poor being most heavily affected. The consequences of this situation are dire, with diarrhoeal diseases causing 842,000 deaths per year, especially in developing countries[10]. Many disease caused by water sanitation are resultant from pathogens that can survive in water or have water-related vectors.

The emergence of new contaminants and newly developed chemical compounds has exposed the downfalls of current water treatment and distribution systems [11], [12]. The ever-increasing rate of worldwide population growth continues to drive up the demand for clean water [13]. Also, climate changes and extended droughts have caused a shift in fresh water distribution,

which has led to inadequate fresh water supply to various regions around the globe [13]. Regions lacking fresh water supplies have made use of other water sources, such as seawater and storm water, to meet their water needs [14]. The use of unconventional water sources for water supply makes it even more important to develop effective treatment methods that clear water of pathogen contamination.

The water treatment technologies currently used are limited and cannot adequately eliminate pathogens from all water sources. Conventional methods for removal of microorganisms from water include oxidation, reduction, ion exchange, precipitation, filtration, electrochemical treatment, chemical treatment, and solvent extraction[15]. However, the use of these conventional techniques are cost prohibitive and do not work efficiently for elimination of low concentrations of microorganisms[16]. Especially in developing countries, funding, governance, and access to appropriate technologies are obstacles to gaining accessible water sanitation systems. This difficulty in overcoming obstacles related to clean water access has raised interest in point-of-use (POU) water treatment methods. Large-scale water treatment systems present many problems to developing countries, such as high cost, need of skilled laborers, and construction complexity. The relatively inexpensive POU water treatment methods avoid these obstacles associated with large-scale water treatment projects.

The development of an efficient POU water treatment technology has become imperative and has led to the interest in nano-enabled technologies for POU approaches. Nanotechnology is recognized as an important area of science and technology that could play a large role in combating the pitfalls of conventional and current POU water treatment devices[17]. It has been suggested that the development of nanotechnology-based POU devices could help developing countries meet their needs for clean water by efficiently providing safe water at a low cost[18].

In recent years, technology has advanced and introduced different types of nanotechnologies to the water industry that may have promising outcomes. The most recent technologies studied to combat microorganism contamination of water sources include nanofiltration membranes, nanoporous ceramics, nanofibers, nanocatalysts, and magnetic nanoparticles [19]. It should be noted, however, that these technologies have yet to prove successful in eliminating *A. baumannii*.

1.3.1. Nanofiltration membranes

Conventional water purification processes, consisting of sedimentation, flocculation, coagulation, and disinfection are not able to remove some organic pollutants, such as small microorganisms[20]. Therefore, filtration membranes play an important role in water purification processes. Currently, various water purification membranes that are used include microfiltration, ultrafiltration, and nanofiltration for water treatment. Membrane processes mentioned above are being incorporated for removal of microorganisms, particulates, and natural organic material from water. These membrane processes are a key component to water purification to ensure that infectious matter, such as bacteria, are not persisting in potable water. Due to the significance of filtration membranes and their role in water purification, research for new materials and water purification technologies is of utmost importance. Currently, researchers are developing nanomaterial-based membranes (i.e. carbon nanotubes, nanoparticles, and dendrimers) in order to contribute to the development of more efficient and cost-effective water filtration processes.

To overcome limitations associated with conventional water treatment systems, a new adsorption technique based on the application of carbon nanotubes (CNTs) has been introduced [21]. CNT-based nanofiltration membranes allow for refinement and optimization of all membrane aspects, such as small and uniformed pore sizes as well as precise control of

membrane reactivity. CNT-based nanofiltration membranes have been shown to have a significantly higher adsorption capacity than conventional purification materials, such as activated carbon [22]. Also, CNTs exhibit shorter equilibrium times [23] and higher adsorption energy [24]. CNT-based membranes are able to effectively adsorb and remove biological contaminants, such as bacteria, from water due to their structural and functional properties. The aggregated mesopores of CNTs provide a large area that can adsorb contaminants the size of bacteria and other pathogens. Also, microbial adsorption on CNTs can occur on four different regions in the CNTs, providing ample space for adsorption. By specifically modifying CNTs for selective adsorption of pathogens, the adsorption kinetics of bacteria on CNTs is almost instantaneous [25]. This type of rapid, selective pathogen adsorption feature is not available when using activated carbon. Also, the selective adsorption feature of CNTs suggests they could be used for other applications, such as microorganism detection.

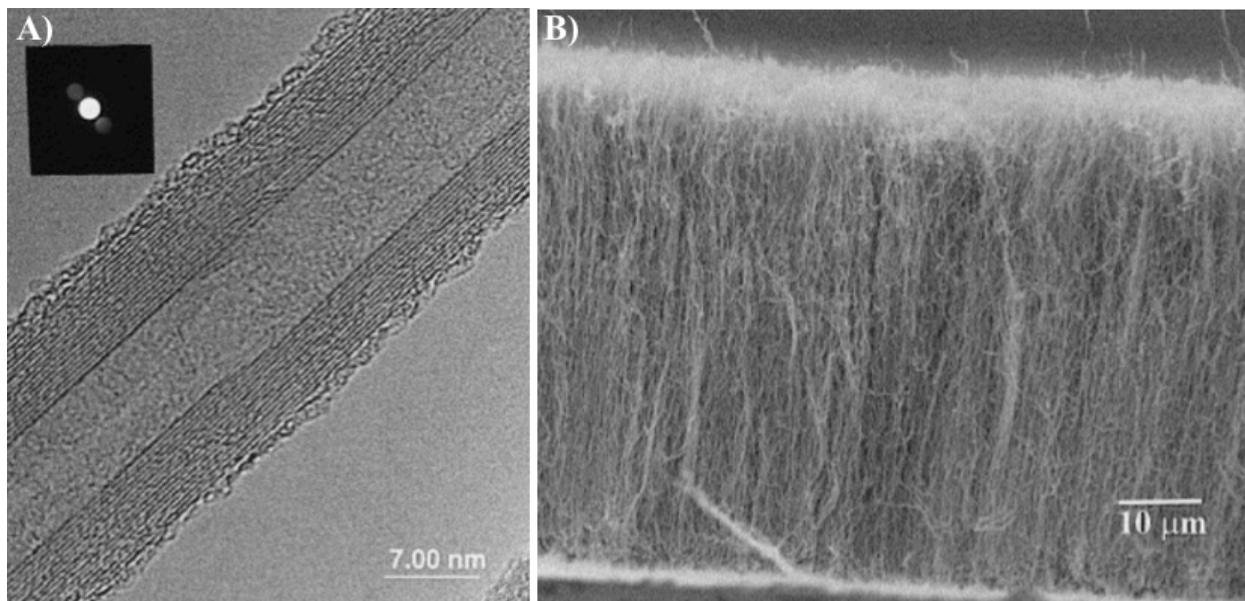


Figure 1.2. Scanning electron microscopy (SEM) image of CNTs. A) SEM image of a single CNT with a multilayered structure. Inset: Electron diffraction spots seen in a typical electron diffraction pattern. B) SEM image of CNTs that were grown on quartz substrate [26].

Although CNTs present many great advantages in the realm of water treatment, various

concerns exist regarding the safety of CNTs. It has been reported that CNTs are toxic and can have a negative impact on the environment [27]. The use of CNT filters for water treatment poses the risk that a portion of media could be lost after repeated usage. Release of toxic CNTs into the environment would not only disrupt the natural ecosystem, but also have very harmful effects on humans if introduced into the body [28], [29]. Entry of CNTs into the human body can cause inflammation, fibrosis, granulomas, and cancer [28]. Clearly, there is still more work to be done before CNTs can be safely used for water treatment purposes. Various groups are currently researching the possibility of developing organic nanotubes for water purification, which are made from various polymers and biomaterials [30], [31]. These technologies could potentially avoid some downsides associated with CNTs.

1.3.2. Nanoporous ceramics

Nanoporous ceramic biomediation filtration techniques have been developed in order to treat contaminated water and convert pollutants into nontoxic substances[32]. For example, MetaMateria Technologies offers nano-enhanced ceramic products with high surface areas and porous structures that can host active materials, such as beneficial aerobic bioremediation colonies. Bioremediation is the application of the natural metabolic ability of microorganisms to transform organic contaminants into less harmful, non-hazardous substances[33]. These nontoxic substances can then be assimilated into natural biogeochemical cycles. The aerobic bioremediation colonies hosted within the porous ceramic material are purported to convert organic pollutants into nontoxic substances. Other research groups have also developed nanoporous ceramic membrane filters designed from ceramic nanopowders on support membranes[34], [35]. These nanoporous ceramic membrane filters can effectively remove various microorganisms from water.

Although nanoporous ceramic filtration systems are more fouling-resistant and chemically stable than polymeric-based water treatment systems, these nanoporous ceramic-based water filtration devices do require maintenance[36]. Some devices require much time to allow the biolayer to establish within the ceramic material prior to use. Also, these devices must be frequently cleaned on the filter's surface.

1.3.3 Nanofibers

Various biotechnologies have also been developed in attempt to overcome the limitations of current water treatment methods. Polysaccharide nanofiber biomaterials have recently been deemed as a very promising option for water purification purposes. Specifically, ultrafine chitosan nanofibers and cellulose nanofibers have been shown to have a high pathogen adsorption capacity in combination with high permeation flux and high rejection rates, compared to commercially available ultrafiltration membranes [37], [38]. These nanofibers are prepared naturally and are not broken down by fabrication processes, allowing them to retain high tensile strength following processing. Also, chitosan nanofibers and cellulose nanofibers are attractive options for water treatment application due to their low toxicity and high potential for surface modifications [38].

Although polysaccharide nanofibers exhibit promising results in terms of water purification, large-scale production of these nanofibers would be very difficult. Corrosive acid/alkali chemicals are used to prepare cellulose and chitin nanofibers, potentially causing a negative environmental impact. Also, functionalizing the surface of nanofibers will prove to be challenging on a large scale due to the problems associated with obtaining uniformity of surface modification and obtaining ultrathin coatings without affecting the filter pore size [39]. Furthermore, low wettability, sparse nanoscale selectivity, and mechanical weakness hinder

nanofiber production on a large scale for water purification applications [40]. These drawbacks will need to be circumvented prior to nanofiber commercialization.

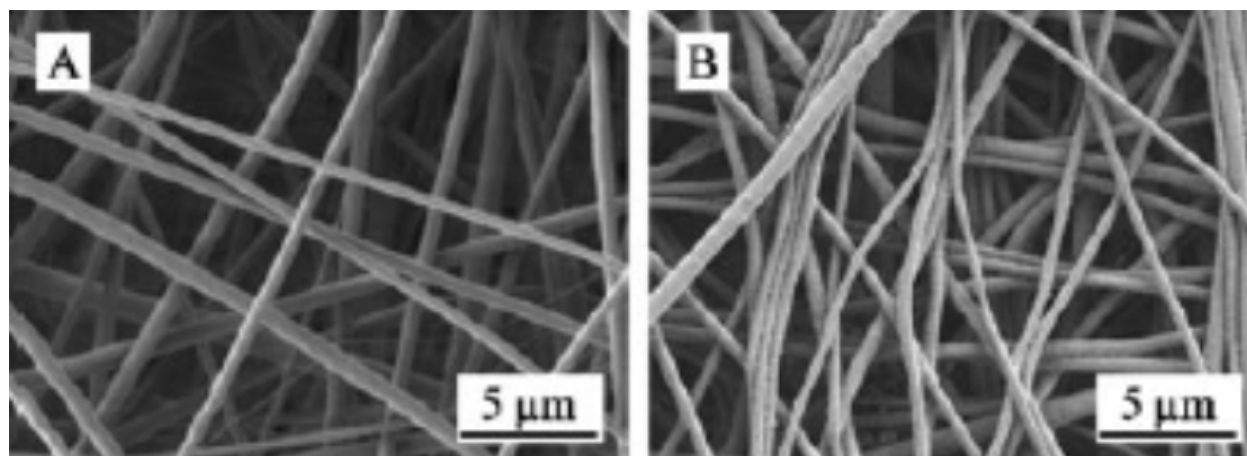


Figure 1.3. Cellulose nanofibers imaged using SEM. A) Cellulose acetate nanofibers. B) Regenerated cellulose nanofibers [41].

1.3.4. Nanocatalysts

Nanoscale semiconductor photocatalytic materials have been deemed as an attractive option for use as water treatment technology[42], [43]. These photocatalytic materials generate reactive oxygen species (ROS) (i.e. H_2O_2 , $\text{OH}\cdot$, $\text{O}_2\cdot^-$, O_3) upon activation, thereby causing the degradation of organics and inactivation of pathogens [44]. Nanoscale titanium dioxide (TiO_2) photocatalysts have gained the most attention as a photocatalyst for water treatment purposes. This photocatalyst is well known for its rapid breakdown of toxins, without generating any secondary pollutants [44]. TiO_2 remains very active and stable following repeated use as a water treatment technology. Many other photocatalysts, such as cadmium sulfide and gallium phosphide, undergo chemical breakdown and emit toxic chemicals following repeated use, unlike TiO_2 .

Researchers have developed methods for functionalizing TiO_2 in order to shift its excitation wavelength to the visible light region, making the material more applicable in the natural environment setting and extending its usefulness in areas lacking electricity. By doping

TiO₂ with certain cationic or anionic materials, the photocatalyst can be activated by sunlight. These types of doped or modified nanoscale TiO₂ photocatalysts have been shown to eliminate bacteria and other various microbes when activated [45]–[48]. The ROS emitted by activated nanoscale TiO₂ photocatalysts break cell membranes and oxidize residual cellular debris [49], thereby making TiO₂ photocatalyst technology a viable option for water purification.

Although nanoscale TiO₂ photocatalysts present many attributes that would be beneficial for water treatment purposes, the applicability of this technology for water treatment still has various hurdles to overcome before possible use. Nanoscale TiO₂ photocatalysts are limited by slow kinetics and they must be continually activated by light exposure for removal of contaminants. Also, the TiO₂ photocatalysts tend to agglomerate during operation, thereby reducing surface area and reusability [44]. Furthermore, the potential release of the compounds coating the surface of TiO₂ photocatalysts could pose a major environmental risk and negatively affect the ecosystem. These limitations hinder the commercialization of nanoscale TiO₂ photocatalysts for water treatment. Another problem to point out is the difficulty in setting up and maintaining nanoscale TiO₂ photocatalyst devices, thereby hindering their usefulness as POU devices.

1.3.5. Magnetic nanoparticles

The nanomaterials previously discussed have drawbacks limiting usability. Limitations of nanofiltration membranes include slow, diffusion-limited operation and surface sites, which decrease the adsorption capacity of the membrane. Nanofiltration membranes can also suffer the consequences of rapid saturation, thereby rendering the membrane nonfunctional. Thus, the development of nanotechnologies with higher adsorptive capacity, low diffusion resistance, and fast separation is of great importance in practical engineering applications.

Recently, magnetic nanoparticles (MNPs) have been suggested as a possible cost-effective and efficient alternative to current water treatment materials. MNPs have a high surface area to volume ratio, which enables high adsorption efficiency and provides a large number of available surface sites. Also, the ability to easily synthesize, functionalize, and control design parameters of MNPs makes them very versatile. Furthermore, the low-toxicity, chemical inertness and biocompatibility of MNPs make them outstanding candidates for water treatment applications. Following water treatment, the adsorbed pollutants on the surface of the MNPs can be removed, allowing for effective reuse of the MNPs[50]. This characteristic makes MNPs more cost effective and a viable possibility for use in designing POU water treatment devices.

Singh et al. have reported that surface-engineered MNPs allow for successful capture and extraction of *Escherichia coli* from PBS [51]. Also, Kang et al. have reported that genetically engineered human opsonin functionalized MNPs can be used to successfully bind and extract *Staphylococcus aureus* or *Escherichia coli* from biological fluid [52]. Unfortunately, very few nanoparticles have been shown to bind *A. baumannii*. Also, many of the nanoparticles developed for bacterial capture are functionalized with genetically engineered, synthetic, or biomacromolecular ligands. Such surface functionalization may pose special challenges in achieving the Food and Drug Administration (FDA) approval required for many important applications. Furthermore, very few reports indicate bacterial capture in less than 1 hour. This is a notable unmet need because rapid extraction of bacteria is essential in order to allow effective decision-making in assessing potential pathogen contamination and to minimize risk of infection.

In order to address the problems of biocompatibility and rapid capture, a new and effective aqueous stabilized surface ligand with low regeneration cost must be engineered. Functionalizing MNPs with biocompatible, bacterial targeting motifs is a technique that can be

employed to significantly improve the efficiency of targeting pathogens in contaminated water. By surface functionalizing MNPs with biorecognition ligands, a large amount of free functional groups are available on the surface and are stable in aqueous solution, which is necessary for the successful adsorption of pathogens[53], [54]. Optimization of the surface ligand for rapid binding would enable the use of superparamagnetic MNPs for rapid removal and high separation efficiency of bacteria from water via the application of a magnetic field. The development of low-cost, bacteria-targeting ligands for MNPs must be further investigated in order to harness the potential of MNPs for application in the field of water treatment. Research in this area is just beginning and studies are needed in order to develop NPs that can be used to purify water on a large scale.

1.4. Aims addressed in this thesis project

Research presented in this thesis is aimed to develop a ligand that can be readily conjugated to nanoparticles for the rapid targeting and binding of *A. baumannii*. The *A. baumannii*-targeting ligand is specifically designed to meet FDA requirements for commercialization purposes. Precise criteria are met to ensure rapid capture of *A. baumannii* in fluid using the ligand-functionalize nanoparticle system. Completion of this work will result in the development of a ligand that can be functionalized to the surface of nanoparticles for the rapid capture and removal of *A. baumannii* from contaminated water, thereby serving as an effective technology for water treatment.

1.4.1. Synthesize and physically characterize colistin-functionalized gold nanoparticles (Col-PEG-AuNPs)

Colistin, a naturally occurring cationic decapeptide isolated from *Bacillus polymyxa* var. *colistinus* [55], is a potent broad-spectrum antimicrobial that was first used in the 1960s. The

cationic colistin molecule and the negatively charged lipid A component of bacterial lipopolysaccharide (LPS) interact both electrostatically and hydrophobically [56], [57], presumably allowing for Col-PEG-AuNP capture of *A. baumannii*. *Objective 1* of this aim is to conjugate colistin to the AuNP surface using a heterobifunctional PEG (polyethylene glycol) linker. Additional thiolated PEG, lacking colistin, will be used to passivate AuNP sites left unoccupied by colistin groups, thereby minimizing nonspecific interactions. *Objective 2* of this aim is to confirm colistin conjugation to the AuNPs and to analyze biocompatibility.

Utilizing colistin as a targeting ligand presents many advantages over synthetic, genetically engineered, or biomacromolecular ligands that have been used in this context [51], [58], [59]. One advantage is that colistin is a readily available, approved antibiotic that has been used in the clinical setting for decades. This design simplifies development and facilitates regulatory considerations relative to the use of genetically engineered or new biomacromolecular ligands.

1.4.2. Evaluate and characterize Col-PEG-AuNP binding with A. baumannii

Following the development of a novel colistin-functionalized nanoparticle, the effects of colistin surface presentation on Col-PEG-AuNPs will be examined. The *in vitro* binding kinetics of Col-PEG-AuNPs with *A. baumannii* will be assessed. *Objective 1* of this aim is to confirm Col-PEG-AuNP association with *A. baumannii*. *Objective 2* of this aim is to determine the rate of nanoparticle association to *A. baumannii*.

1.5. Organization of Thesis

Several studies will be performed to evaluate the efficacy of the conjugation method used to functionalize AuNPs with colistin. Also, various studies will be employed to analyze NP binding to *A. baumannii*. Chapter 2 will describe the methods of analysis used to evaluate NP

synthesis and *A. baumannii* binding kinetics. Chapter 3 contains the results and discussion obtained from the various studies presented in Chapter 2.

CHAPTER 2

Materials and Methods

2.1. Materials

All materials were obtained from Sigma-Aldrich (St Louis, MO, USA) and used as received unless otherwise noted.

2.2. Methods

2.2.1. Synthesis of Col-PEG-AuNPs

Col-PEG-AuNPs were prepared using a multistep approach

(i). *Conjugating Colistin to NHS-PEG₃₄₀₀-OPSS tethers.* Colistin was suspended in 100 mM sodium bicarbonate (NaHCO₃) (pH 8.5) at a concentration of 0.29 mg/mL. NHS-PEG₃₄₀₀-OPSS (succinimidyl ester-polyethylene glycol-ortho-pyridyl disulfide, Laysan Bio, Inc., Arab, AL, USA) was prepared in 100 mM NaHCO₃ at a concentration of 3.19 mg/mL. 900 μ L of NHS-PEG₃₄₀₀-OPSS solution was added in drop-wise fashion to 9 mL of colistin solution. The solution was vortexed for 10 seconds and then allowed to react at 4°C for 2 h.

(ii). *Attachment of Colistin-PEG₃₄₀₀-OPSS onto AuNPs.* 1.425 mL of Colistin-PEG₃₄₀₀-OPSS from step (i) and an additional 75 μ L of 100 mM NaHCO₃ solution were added to 15 mL of 20 nm AuNP suspension (Ted Pella Inc., Redding, CA, USA). The solution was incubated at 25°C for 1 h.

(iii). *Passivation of Col-PEG-AuNPs with HS-mPEG₂₀₀₀.* 109 μ M HS-mPEG₂₀₀₀ (thiol-polyethylene glycol, Laysan Bio, Inc.) was prepared in distilled water. 1.5 mL of 109 μ M HS-mPEG₂₀₀₀ solution was added to the Col-PEG-AuNPs resultant from step (ii), and then incubated

at 25°C for 1 h. Following incubation, the functionalized nanoparticles were centrifuged at 8,000g for 30 minutes. The supernatant was decanted and particles were resuspended in 70% ethanol. The solution was stored at 4°C for 24 h.

2.2.2. Synthesis of polyethylene glycol-functionalized gold nanoparticles (PEG-AuNPs)

PEG-AuNPs were prepared in three steps

(i). *Dilution of NHS-PEG₃₄₀₀-OPSS.* NHS-PEG₃₄₀₀-OPSS was prepared in 100 mM NaHCO₃ (pH 8.5) at a concentration of 3.19 mg/mL. 900 µL of NHS-PEG₃₄₀₀-OPSS solution was added in drop-wise fashion to 9 mL of 100 mM NaHCO₃ solution. The solution was vortexed for 10 seconds and then stored at 4°C for 2 h.

(ii). *Attachment of NHS-PEG₃₄₀₀-OPSS onto AuNPs.* 1.425 mL of NHS-PEG₃₄₀₀-OPSS solution from step (i) and an additional 75 µL of 100 mM NaHCO₃ solution were added to 15 mL of 20 nm AuNP suspension. The solution was incubated at 25°C for 1 h.

(iii). *Passivation of PEG-AuNPs with HS-mPEG₂₀₀₀.* 109 µM HS-mPEG₂₀₀₀ was prepared in distilled water. 1.5 mL of 109 µM HS-mPEG₂₀₀₀ solution was added to the PEG-AuNPs resultant from step (ii), and then incubated at 25°C for 1 h. Following incubation, the functionalized nanoparticles were centrifuged at 8,000g for 30 minutes. The supernatant was decanted and particles were resuspended in 70% ethanol. The solution was stored at 4°C for 24 h.

2.2.3. Physical characterization of Col-PEG-AuNPs and PEG-AuNPs

Unconjugated AuNPs, Col-PEG-AuNPs, and PEG-AuNPs were centrifuged at 8,000g for 30 minutes. The supernatant was decanted and particles were resuspended in nanopure water at a NP concentration of 0.5 mM. Droplets of diluted, aqueous NP suspensions were deposited on carbon film-backed copper grids (Ted Pella Inc.) and blotted dry. Samples were left to dry for 2

h at 25°C prior to imaging on a STEM operating at 200 kV (FEI Tecnai Osiris, Hillsboro, OR, USA) in transmission electron microscope (TEM) mode. X-rays emitted from the specimens were collected via a solid-state detector and recorded to form EDS spectrums using ESPRIT imaging software (Bruker, Billerica, MA, USA). The specific energies of the EDS emission peaks were used to identify elements within each sample.

2.2.4. Confirmation of Colistin-PEG₃₄₀₀-OPSS and NHS-PEG₃₄₀₀-OPSS conjugation to AuNPs

Zeta potential measurements and size measurements were obtained with a Malvern Instruments Zetasizer (Malvern Nanosizer ZS, Malvern Instruments, U.K.) to determine surface charge and size of the Col-PEG-AuNPs, PEG-AuNPs, and unconjugated AuNPs. Each NP formulation was resuspended in dH₂O (pH 7.5) at an AuNP concentration of 1.0 mM, respectively.

H¹ NMR spectroscopy was used to confirm colistin conjugation to the Col-PEG-AuNPs. All H¹ NMR spectrums were recorded in deuterium oxide (D₂O), pH 7.4 using a Bruker 600 MHz spectrometer (Bruker, 600 MHz, Billerica, MA, USA). Col-PEG-AuNPs at a NP concentration of 5 mM were lyophilized for 24 h. The sample was resuspended in D₂O and then centrifuged at 8,000g for 30 min. The supernatant was decanted and analyzed using H¹ NMR spectroscopy, prior to the iodination process described below.

The sample pellet was resuspended in D₂O and five iodine crystals were added. The iodinated Col-PEG-AuNP sample was vortexed for 10 s, every 20 min, for the total duration of 1 h. Iodine is a nucleophile and, therefore, attacks sulfhydryl groups present in the OPSS-containing ligand [60]. During this reaction, nucleophilic substitution of iodine with a thiol takes place, thereby causing quantitative decoupling of the OPSS-containing ligands from the surface of the AuNPs. Iodination of AuNPs reduces their aqueous solubility and forces them to

spontaneously precipitate [61], leaving only OPSS-containing ligand and iodine in the supernatant.

Following 1 h of periodic vortexing, the sample was stored at 4°C for 24 h to allow the iodine crystals to settle at the bottom of the suspension. Then, only Colistin-PEG₃₄₀₀-OPSS ligand remained in suspension and was extracted for analysis using ¹H NMR spectroscopy. The same procedure was used to analyze the NHS-PEG₃₄₀₀-OPSS ligand of the PEG-AuNPs. Also, free colistin (6.5 mM) in D₂O was analyzed using ¹H NMR spectroscopy.

2.2.5. Cell culture

HepG2 cells (human liver carcinoma cancer cell line) were cultured in Dulbecco's modified Eagle's medium (DMEM, Gibco Cell Culture, Carlsbad, CA, USA) supplemented with 10% fetal bovine serum (FBS, Gibco) at 37°C in a humidified atmosphere containing 5% CO₂. HUVEC cells (human umbilical vein endothelial cell line) were cultured in vascular basal cell medium (ATCC PCS-100-300, Manassas, VA, USA) supplemented with endothelial cell growth kit-VEGF (ATCC PCS-100-41) at 37°C in a humidified atmosphere containing 5% CO₂.

2.2.6. In vitro cytotoxicity studies

The cytotoxicity induced by Col-PEG-AuNPs, PEG-AuNPs, and free colistin on mammalian cell cultures was determined using the alamarBlue (Invitrogen Co., Carlsbad, CA, USA) assay [62]. HepG2 and HUVEC cells were seeded in clear, flat 96-well plates at a density of 10,000 cells/well in 200 µL of medium and incubated for 24 h at 37°C. Next, culture medium was removed and exchanged with medium containing fresh Col-PEG-AuNPs and PEG-AuNPs at concentrations of 2, 1, 0.5, 0.25, and 0 mM, respectively. Cells were also treated with free colistin at concentrations of 900, 90, 70, 15, 1 and 0 µM. After incubation for 24 h at 37°C, cells were washed three times with phosphate buffer solution (PBS), pH 7.4 and treated with 200 µL

of alamarBlue containing media. Cells were then incubated for an additional 4 h at 37°C.

Fluorescence was quantified using a plate-reader (Tecan, Infinite M1000 Pro, Switzerland), with an excitation wavelength of 540 nm and emission wavelength of 590 nm.

2.2.7. *In vitro* hemocompatibility

Human whole blood was collected from anonymous, consenting human donors in accordance with an approved Institutional Review Board (IRB) protocol (IRB 111251). Red blood cells (RBCs) were isolated according to well-established protocols [63]. Four different concentrations (2, 1, 0.5, 0.25, and 0 mM) of Col-PEG-AuNPs and PEG-AuNPs were prepared in PBS, pH 7.4, respectively. Free colistin (900, 0.9, 0.4, 0.2, and 0 μM) was also prepared in PBS, pH 7.4. Col-PEG-AuNPs, PEG-AuNPs, and free colistin were incubated with RBCs for 1h at 37°C, each respectively, at the concentrations outlined above. Following incubation, the samples were centrifuged and the supernatant was spectrophotometrically analyzed for hemoglobin release using a plate-reader (Tecan, Infinite M1000 Pro) at 451 nm in order to determine percent hemolysis relative to the positive control (Triton X-100 detergent). The negative control used was PBS, pH 7.4. Percent of hemoglobin release was calculated according to the following equation:

$$\text{Hemoglobin release \%} = \frac{(\text{Sample}_{451 \text{ nm}} - \text{Negative control}_{451 \text{ nm}})}{(\text{Positive control}_{451 \text{ nm}} - \text{Negative control}_{451 \text{ nm}})} * 100\%$$

2.2.8. *A. baumannii* binding

A. baumannii (17978) was grown in Luria Bertani (LB) broth at 37°C, 200 rpm until reaching late log phase. *A. baumannii* cultures (5×10^8 CFU/ml, pH 7.4) were exposed to Col-PEG-AuNPs (1 mM NPs) for 1 hour at 37°C, 200 rpm prior to centrifugation at 8,000g for 20 min to pellet the cells. The supernatant was discarded, and the cells were washed two times with sterile dH₂O prior to STEM imaging. To fix the cells, 2% formaldehyde was added, and the

samples were incubated for 30 min at 25°C. Droplets of Col-PEG-AuNP bacteria suspension were deposited on carbon film-backed copper grids (Ted Pella Inc.) and blotted dry. Samples were left to dry for 2 h at 25°C prior to imaging on a STEM operating at 200 kV (FEI Tecnai Osiris) in STEM mode. The same procedure was repeated using PEG-AuNPs. X-rays emitted from the specimens were collected and recorded to form EDS spectrums using ESPIRIT imaging software, allowing for elemental analysis.

2.2.9. AuNP standard concentration curve

The concentration of AuNPs was quantified using absorbance techniques, from which a standard concentration curve was generated. AuNPs were resuspended in PBS, pH 7.4 and diluted to various concentrations (2.0, 1.5, 1.0, 0.75, 0.5, 0.25, 0.12, 0 mM). 200 µL of each sample was plated in a 96-well plate. Absorbance was quantified using a plate-reader (Tecan, Infinite F500, Switzerland), with an absorbance wavelength of 492 nm. A standard concentration curve was generated from the data and is shown in the Appendix as Figure S5.

2.2.10. *A. baumannii* binding kinetics

The rate of nanoparticle association to *A. baumannii* was analyzed using a spin filtration/absorbance technique. Initially, *A. baumannii* was grown in LB at 37°C, 200 rpm until reaching late log phase. *A. baumannii* diluted in PBS, pH 7.4 (5×10^8 CFU/ml) was then exposed to Col-PEG-AuNPs (1 mM) and PEG-AuNPs (1 mM), respectively, for various times (0, 5, 10, 20, 30, 60, 120 min) prior to centrifugation at 4,900g for 1 min to pellet all of the bacteria, including the nanoparticle-bound bacteria. 200 µL of the supernatant, which now contained only nanoparticles, was plated in a 96-well plate. Absorbance was quantified using a plate-reader (Tecan Infinite F500), with an absorbance wavelength of 492 nm. Results were then compared to the AuNP standard concentration curve (2.2.9.) in order to determine the concentration of

nanoparticles unbound to bacteria. From this, the number of nanoparticles bound to bacteria was estimated.

2.2.11. Statistical analysis

All experiments were performed in triplicate. The results were expressed as the arithmetic mean \pm standard deviation (SD). Samples were compared by one-way analysis of variance (ANOVA). A *post hoc* comparison test was utilized to discriminate between groups of means. The factor was declared significant if the probability of the null hypothesis was $< 5\%$ (*p-value* < 0.05).

2.2.12. Ethical compliance

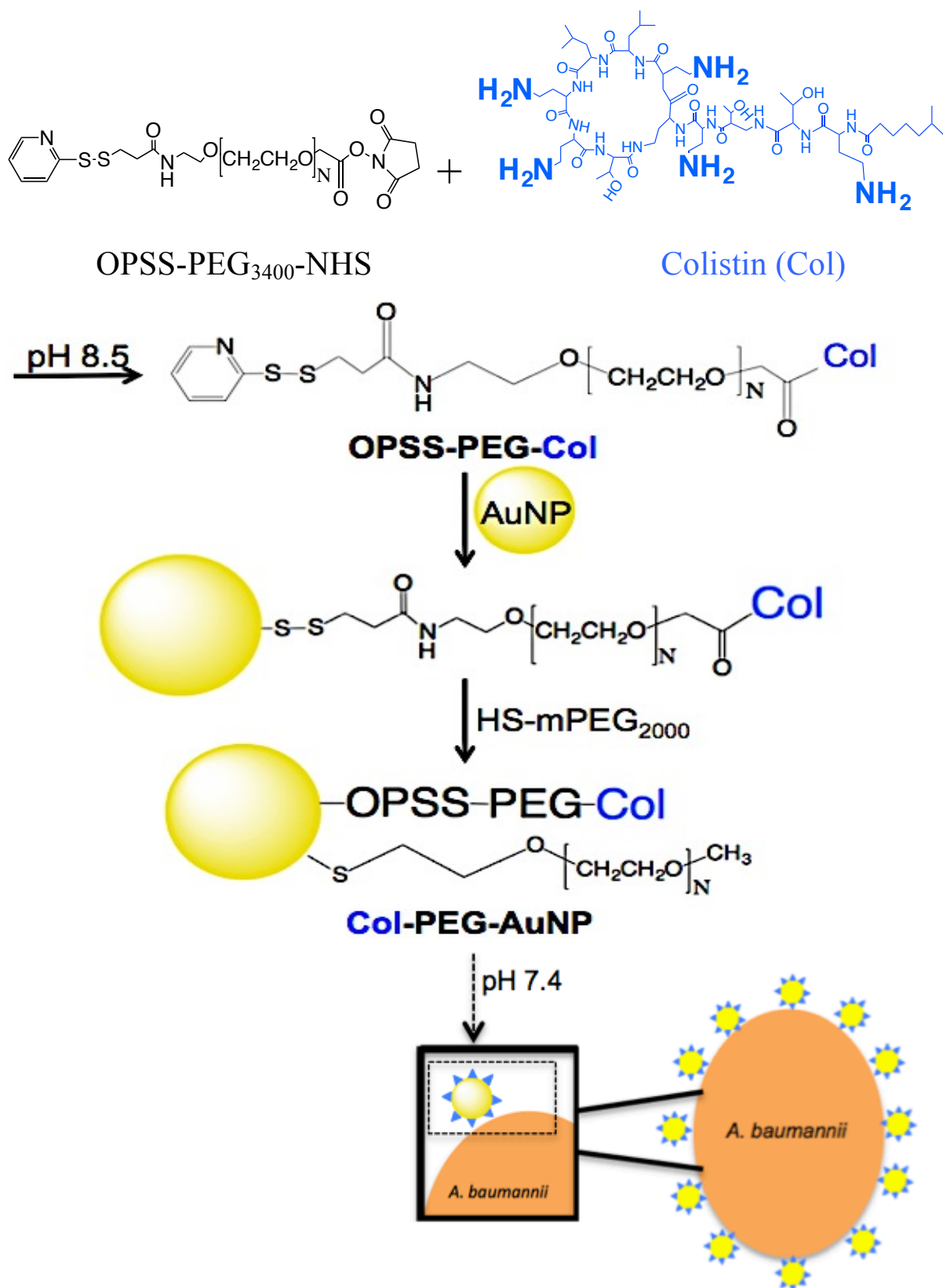
Human whole blood was collected from anonymous donors in accordance with an approved IRB protocol (IRB 111251).

CHAPTER 3

Results

3.1. Preparation of Col-PEG-AuNPs and PEG-AuNPs

Colistin was tethered to AuNP surfaces using heterobifunctional PEG, as depicted in Scheme 1. NHS was used to couple the PEG group to any single, equivalently reactive amine residue of colistin. Upon entering an aqueous environment, the NHS groups of the NHS-PEG₃₄₀₀-OPSS linker covalently bind to the amine groups of the colistin antibiotic via carbodiimide chemistry, resulting in amide bonds [64], [65]. The sulfur groups of the OPSS end of the heterobifunctional PEG have a strong affinity for the gold surfaces of the AuNPs. Therefore, use of the PEG heterobifunctional linker enabled colistin decoration of the AuNP with a PEG molecular spacer, which was designed to reduce steric hindrance of colistin binding to bacteria. Thiolated PEG (HS-PEG₂₀₀₀) was used to passivate the AuNP surface unoccupied by the Colistin-PEG₃₄₀₀-OPSS. This additional PEG was intended to further passivate the Col-PEG-AuNPs, reduce nonspecific binding onto the gold surface, and sterically stabilize the NPs in both biological and non-biological fluids. In the range of physiological pH values, between pH 7.0 and 8.5, the primary amine groups of colistin were protonated, and, therefore, positively charged [66], [67]. The positive charge of colistin allowed for binding to the negatively charged outer membrane of *A. baumannii* [56]. PEG-AuNPs were synthesized using a very similar, multistep approach, and used as a control group that lacked colistin decoration.



Scheme 1. Synthesis scheme of Col-PEG-AuNP and schematic of interaction between Col-PEG-AuNPs and *A. baumannii*.

3.2. Characterization of functionalized AuNPs

TEM images consisted of highly mono-disperse NPs, as shown in Figure 3.1, with an average NP core size of 23.2 nm. The EDS capabilities of the TEM confirmed the presence of gold in the core by characteristic X-rays at 2.120, 9.712, and 11.442 eV (see Fig. S1 in Appendix).

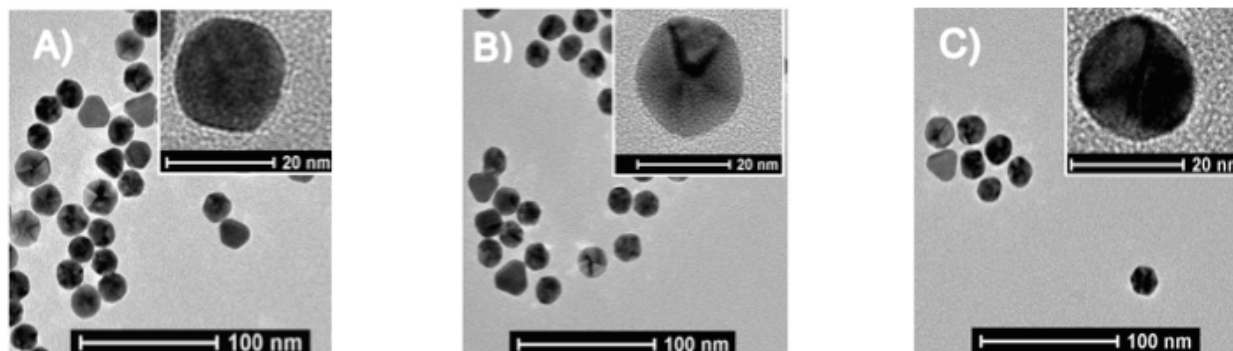


Figure 3.1. TEM, representative images of nanoparticles. A) AuNP, B) PEG-AuNP, C) Col-PEG-AuNP

3.3. Confirmation of Colistin-PEG₃₄₀₀-OPSS and NHS-PEG₃₄₀₀-OPSS conjugation to AuNPs

The successful conjugation of Colistin-PEG₃₄₀₀-OPSS and NHS-PEG₃₄₀₀-OPSS to AuNPs was confirmed through zeta potential, size, and H¹ NMR spectroscopy measurements. The zeta potential of Col-PEG-AuNPs was significantly greater than control PEG-AuNPs or untreated AuNPs (Table 3.1). This increase in zeta potential was consistent with decoration of the AuNPs with strongly cationic colistin.

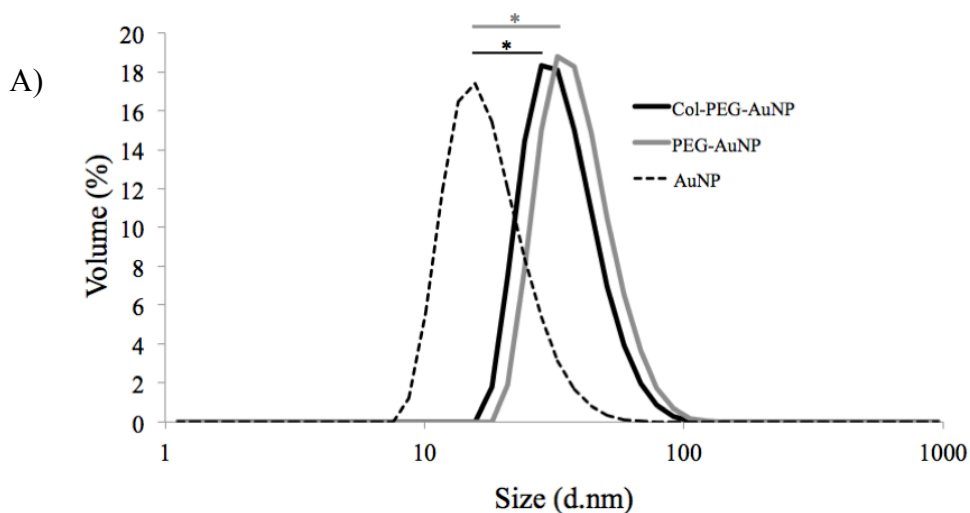
Table 3.1: NP Zeta Potentials (ζ)	
Sample	ζ (mV)
AuNP	-42.8 \pm 2.1
PEG-AuNP	-26.1 \pm 2.5*
Col-PEG-AuNP	-6.37 \pm 1.2*

Table 3.1. Functionalization of AuNPs with NHS-PEG₃₄₀₀-OPSS or Colistin-PEG₃₄₀₀-OPSS significantly increased AuNP zeta potential towards more positive values. ANOVA and *post hoc* analysis prove that both Col-PEG-AuNP and PEG-AuNP zeta-potentials are significantly different than AuNP zeta-potential. Also, Col-PEG-AuNP and PEG-AuNP zeta-potentials are significantly different comparatively. * $p < 0.05$

Passivating the AuNPs through PEGylation alone reduced the zeta potential of untreated AuNPs, presumably due to the partial shielding of the original surface charge. The addition of colistin to the Col-PEG-AuNPs further increased the zeta potential, presumably due to the colistin molecule corona, which is cationically charged at physiological pH values.

Size measurements of the PEG-AuNPs and Col-PEG-AuNPs (Fig. 3.2A) supported ligand conjugation to the AuNPs and allowed an estimation of ligand length. The Colistin-PEG₃₄₀₀-OPSS ligand was approximately 8.5 nm in length when bound to AuNPs, based on a diameter that was roughly 17 nm larger than that of unconjugated AuNPs. Conjugation of NHS-PEG₃₄₀₀-OPSS had a similar effect on size, thereby providing further confidence of the successful generation of PEG-AuNPs.

The hydrodynamic radii of Col-PEG-AuNPs were smaller than those of PEG-AuNPs, as reported by DLS (Fig. 3.2B). Attraction of the positively charged colistin molecules to the negatively charged AuNP surface was presumed to change the PEG linker conformation, resulting in the observed decrease in ligand length, relative to PEG-AuNPs that have a much greater negative zeta potential.



B)

Sample	Size (d.nm)
AuNP	23.3±1.2
PEG-AuNP	45.3±2.3*
Col-PEG-AuNP	39.4±2.5*

Figure 3.2. Functionalization of AuNPs with NHS-PEG₃₄₀₀-OPSS or Colistin-PEG₃₄₀₀-OPSS significantly increased AuNP size. A) Nanoparticle diameter was estimated by DLS. B) Mean size of each nanoparticle. ANOVA and *post hoc* analysis prove that both Col-PEG-AuNP and PEG-AuNP size are significantly different than AuNP size. Also, Col-PEG-AuNP and PEG-AuNP size are significantly different comparatively. * $p < 0.05$

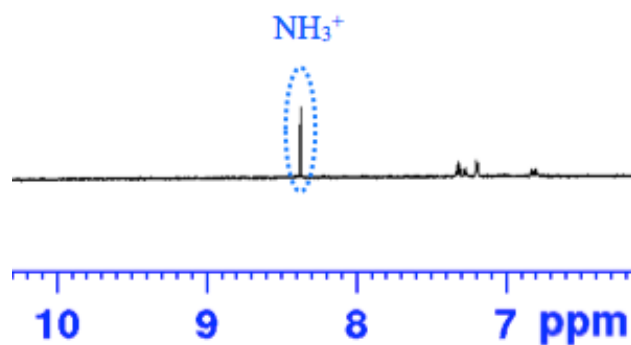
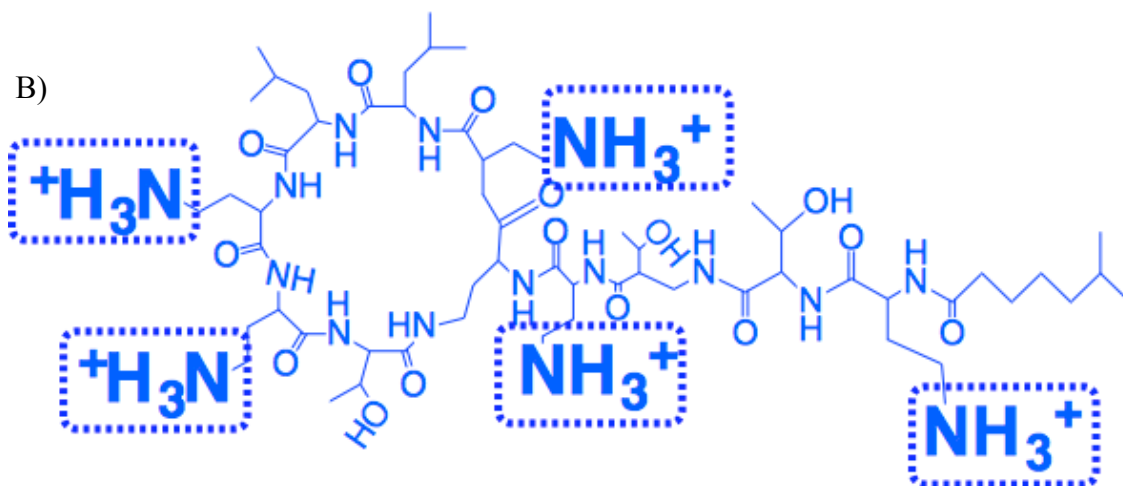
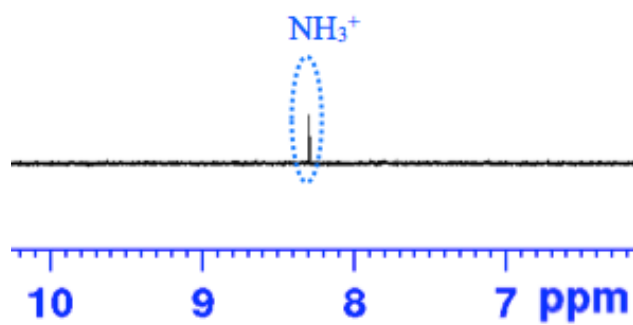
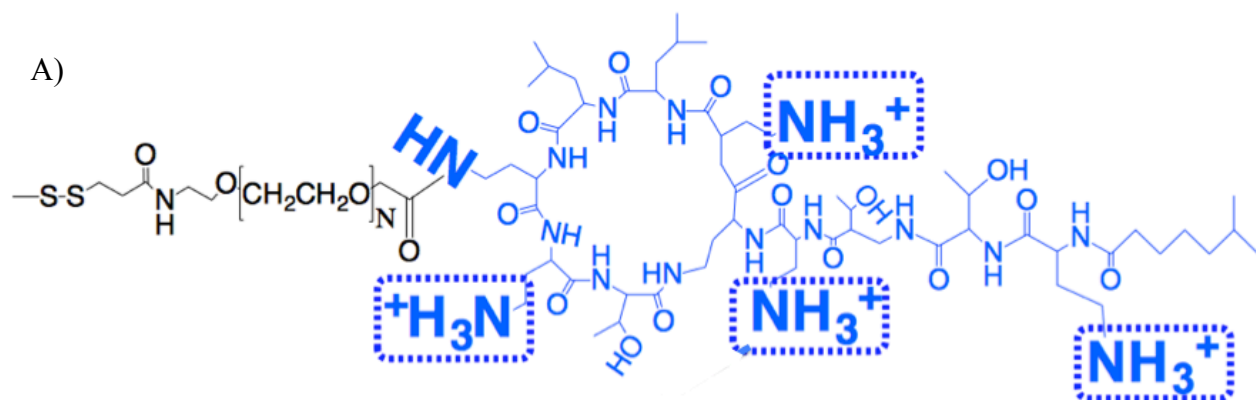
H^1 NMR spectroscopy confirmed conjugation of colistin to the AuNPs (Fig. 3.3A). The Colistin-PEG₃₄₀₀-OPSS ligands were treated with iodine to decouple the ligands from the AuNP surface and then measured using H^1 NMR [68]. This decoupling approach was utilized in order to prevent peak broadening due to the presence of AuNPs in the sample.

H^1 NMR results are shown in Figure 3.3, with the supernatant from iodine treated Col-PEG-AuNPs shown in Figure 3.3A and free colistin shown in Figure 3.3B. The protonated amine groups of colistin are identifiable in both spectrums (Fig. 3.3A, 8.31ppm; 3.3B, 8.38 ppm), consistent with successful conjugation of colistin to the AuNPs. Conjugation of colistin to the

PEG₃₄₀₀-OPSS linker was expected to cause diamagnetic shielding, increasing the electron density surrounding the colistin molecule. The physical shift of the protonated colistin amine peak upfield, as seen by comparing Figure 3.3A to Figure 3.3B, is consistent with diamagnetic shielding and is further evidence that the colistin was bound to the PEG₃₄₀₀-OPSS linker.

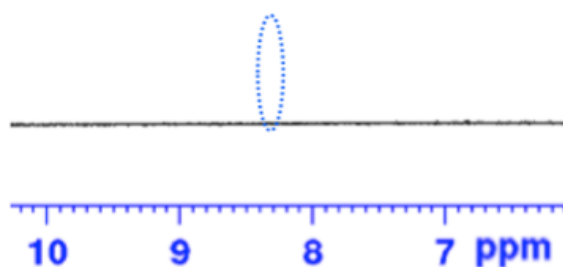
The supernatant of Col-PEG-AuNPs without the addition of iodine was also analyzed using H¹ NMR (Fig. 3.3C) to estimate the amount of colistin containing molecules that were not particle bound. The relative gain and number of counts taken to generate the H¹ NMR spectrum of the non-iodinated Col-PEG-AuNP sample were scaled to allow direct comparison to the iodinated Col-PEG-AuNP H¹ NMR spectrum.

Due to the absence of a protonated amine peak (8.31 ppm) in the H¹ NMR spectrum of non-iodinated Col-PEG-AuNP (Fig. 3.3C), it was estimated that 100% of total colistin was particle bound. Stoichiometry of the reaction and H¹ NMR data support a concentration of colistin bound to particles of 15 μM colistin/mg AuNP, or 3500 colistin ligands per AuNP. This reflects approximately 95% of total AuNP surface coverage, based on a 0.35 nm² PEG footprint area [69]. This was the maximum number of colistin containing ligands that could be loaded onto the surface of a single AuNP while remaining water dispersible. The H¹ NMR spectrum of iodine treated PEG-AuNPs is shown in Figure 3.3D. It can be seen that no signal was present at 8.31 ppm, indicating the absence of colistin in the sample.



C)

**Absence of protonated amine peak
in supernatant, indicating all colistin
bound to AuNP**



D)

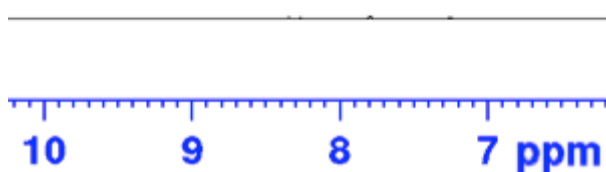
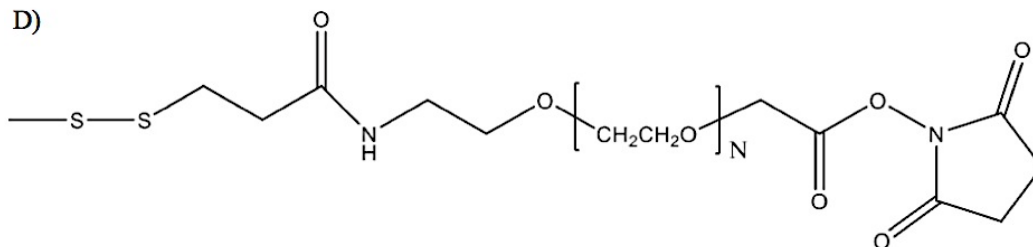


Figure 3.3. H^1 NMR spectrum of (A) iodinated Col-PEG-AuNP supernatant verified that approximately 100% of colistin-containing molecules were bound to AuNPs. A) Supernatant of iodinated Col-PEG-AuNPs. The peak indicated at 8.31 ppm was assigned to the protonated amine groups of colistin. The presence of protonated amine groups in (A) confirmed successful colistin conjugation. B) Free colistin. The peak indicated at 8.38 ppm was assigned to the protonated amine groups of colistin. C) Supernatant of pelleted, non-iodinated Col-PEG-AuNPs. No peak was present at 8.31 ppm, indicating the absence of colistin in the supernatant. D) Supernatant of iodinated PEG-AuNPs. No peak was present at 8.31 ppm, indicating a colistin concentration lower than the limit of detection.

3.4. In vitro cytotoxicity studies

AlamarBlue is a cell membrane-permeable dye that both changes fluorescent properties and color in response to a chemical reduction caused by cell metabolic activity [70]. With AlamarBlue it is possible to compare control group cell viability against experimental group cell viability, from which cytotoxicity can be analyzed quantitatively. After a 24 h incubation period, the cell viability of mammalian cells treated with Col-PEG-AuNPs or PEG-AuNPs was no different than untreated cells (Ctrl) (Fig. 3.4A, 3.4B).

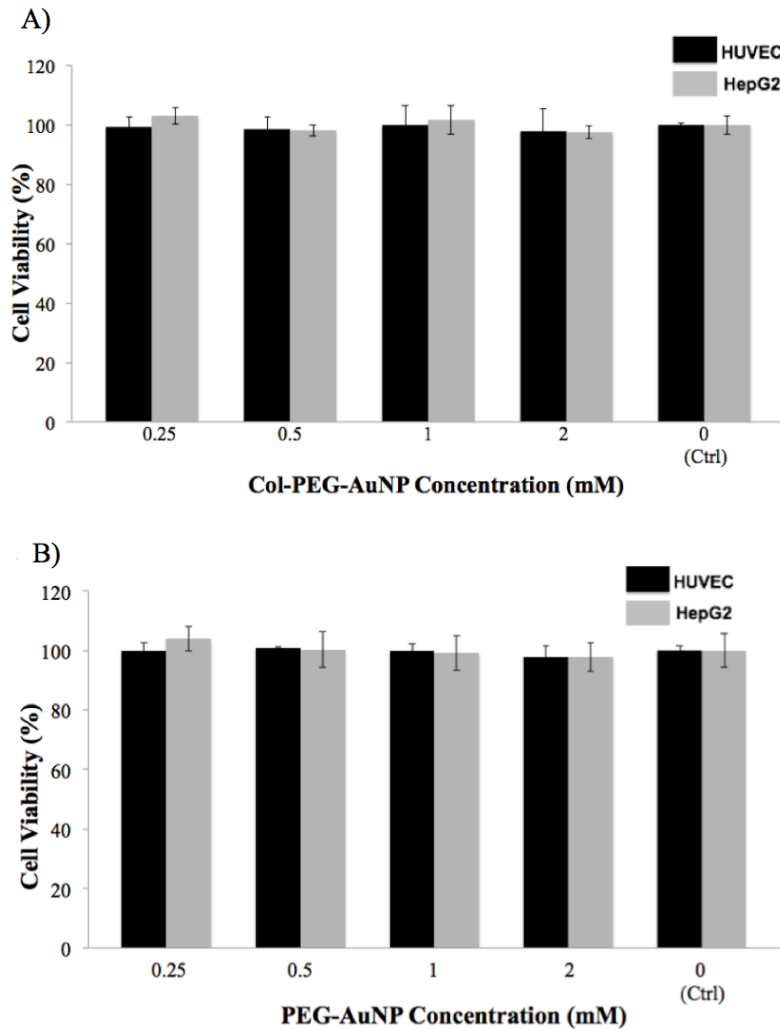


Figure 3.4. (A) Col-PEG-AuNPs and (B) PEG-AuNPs demonstrated cellular compatibility with HUVEC and HepG2 cells. HUVEC and HepG2 cells were treated with different nanoparticle formulations at various concentrations. A) HUVEC and HepG2 cell viability was quantified by the alamarBlue viability assay following 24 h treatment with Col-PEG-AuNPs. B) HUVEC and HepG2 cell viability was quantified by the alamarBlue viability assay following 24 h treatment with PEG-AuNPs. Treatment with Col-PEG-AuNPs or PEG-AuNPs did not cause cell toxicity. Data were normalized to control cells (Ctrl, 0.0), and are shown as mean \pm SD ($n = 3$). (p -values not significant)

Free colistin cytotoxicity was also evaluated *in vitro* using HepG2 and HUVEC mammalian cell lines with alamarBlue [62]. Cell viability above 90% was observed with free colistin concentrations less than 90 μ M. In comparison, cell viability of only about 80% was observed for free colistin at a concentration of 900 μ M (Fig. 3.5). The intravenous colistin

dosage recommended in the United States for sepsis treatment is 5 mg per kilogram (kg) of body weight [71]. Based on the average adult weight of 80 kg in the United States and blood volume of 5 liters, this dose, confined to the 5-liter blood volume of an average adult, results in an initial colistin concentration of 70 μM . 5 mg/kg of colistin, distributed in the 52 liters of water of the average 80 kg human (65% water) [72], results in a colistin concentration of 6.7 μM . The maximum low toxicity colistin dosage administered to cell cultures (90 μM) was consistent with the upper and lower bounds of colistin concentrations administered in clinically approved treatments.

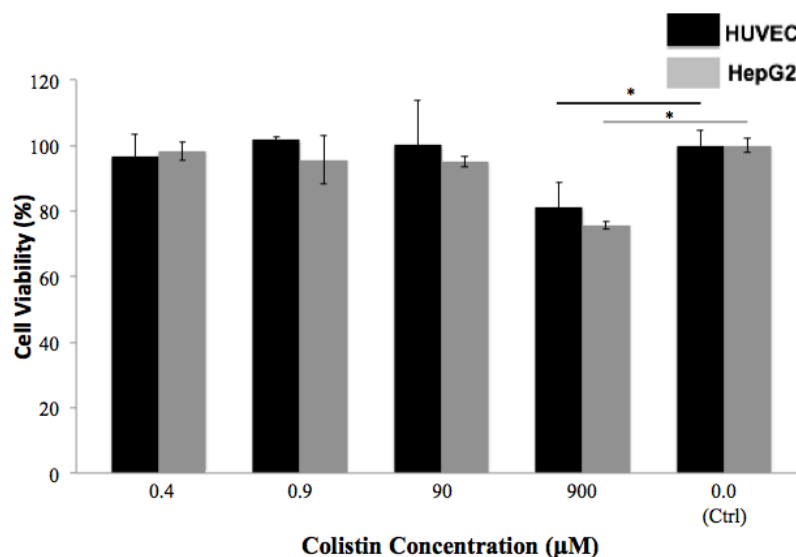


Figure 3.5. Cellular toxicity was not induced by free colistin at concentrations less than 90 μM . HUVEC and HepG2 cell viability was quantified by the alamarBlue viability assay following 24 h treatment with colistin. Treatment with colistin caused cellular toxicity at a colistin concentration of 900 μM in both cell types. Data were normalized to control cells (Ctrl, 0), and are shown as mean \pm SD ($n = 3$). $*p < 0.05$ compared to Ctrl.

3.5. *In vitro* hemocompatibility

Avoiding destabilization and nonspecific interactions with cells and other blood components is key to general hemocompatibility and important for future applications of these materials in contact with blood. A design goal was to maximize the allowable duration for blood

contact time with NPs in order to allow for passive bacterial association or active bacterial targeting by intact, bioactive NPs. *Ex vivo* experiments in human whole blood were done to measure nonspecific RBC interactions and the stability of AuNPs. After 1 h incubation in a solution of isolated RBCs, Col-PEG-AuNPs, PEG-AuNPs, and free colistin were retained in the serum fraction and did not cause hemolysis (Appendix Table S1 and Table S2). PEGylation improves hemocompatibility of similarly sized NPs [73], and we hypothesized that surface PEGylation could be an avenue to further enhance stability. The PEGylation design presumably contributed to the observed lack of adverse interactions between blood cells and Col-PEG-AuNPs. Greater opportunity for Col-PEG-AuNP interaction with *A. baumannii* is one consequence of the extended allowable blood contact time exhibited by these NPs.

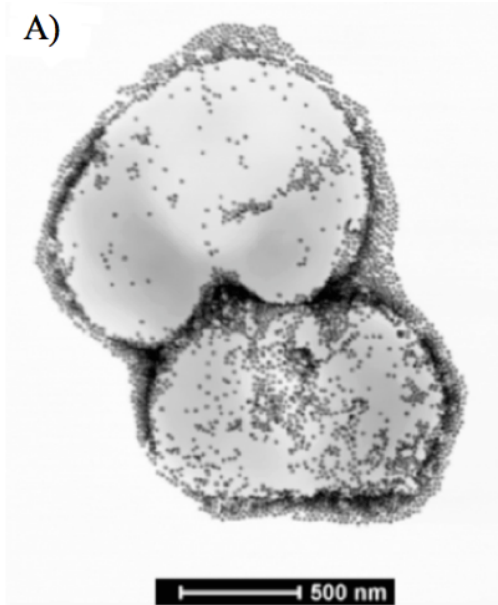
3.6. Nanoparticle binding to *A. baumannii*

The primary component of the outer membrane of Gram-negative bacteria, including *A. baumannii*, is LPS. LPS is composed of lipid A, a core oligosaccharide, and an outer polysaccharide. Lipid A is the innermost aspect of the LPS, as well as the most conserved component of the structure [74]. The proposed binding mechanism between colistin and *A. baumannii* involves lipid A. At physiological pH values, the primary amine groups of the colistin heptapeptide ring and fatty acid tail become protonated, thereby allowing electrostatic interactions with the negatively charged phosphate groups of lipid A [56]. Initial electrostatic interaction between colistin and *A. baumannii* leads to hydrophobic interaction between the fatty acid tail of colistin and the acyl chains of lipid A [57]. The conjugation chemistry of Colistin-PEG₃₄₀₀-OPSS was designed to preserve and protect the molecular characteristics of colistin that are responsible for antibiotic activity and binding to *A. baumannii*. Conjugation of colistin to the heterobifunctional PEG was hypothesized to use a single amine group of the colistin

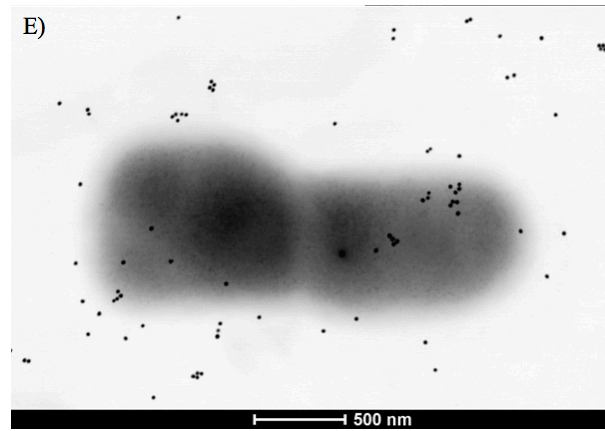
heptapeptide ring. This colistin conformation leaves the fatty acid tail of colistin uninhibited and free to interact with the lipid A on the surface of *A. baumannii*.

Col-PEG-AuNPs associated with the cell wall of *A. baumannii*, as imaged by STEM (Fig. 3.6A). High-angle annular dark-field (HAADF)-EDS analysis of Col-PEG-AuNPs association with *A. baumannii*, Figure 3.6B, verified that gold (Au) and nitrogen (N) were present in the EDS spectrum (see Fig. S2 of Appendix), thereby confirming the presence of Col-PEG-AuNPs and bacteria [75], [76]. In the HAADF-EDS image shown in Figure 3.6B, contrast is directly related to atomic number. This allowed for identification of chemical elements present in the sample. In this case, gold was pseudocolored to identify the Col-PEG-AuNPs (Fig. 3.6C), whereas nitrogen was pseudocolored to identify the bacteria (Fig. 3.6D). Further analysis of Figure 3.6B provided the complete elemental make-up of the *A. baumannii* (Figure S3 of the Appendix). Figures 3.6A and 3.6B suggest that Col-PEG-AuNPs attached to the surface of *A. baumannii*. PEG-AuNPs did not bind to the bacterial surface (Fig. 3.6E), confirming that colistin is an effective targeting ligand. The HAADF-EDS image shown in Figure 3.6F allowed for identification of chemical elements present in the sample. The EDS spectrum (see Fig. S4 of Appendix) verified the presence of bacteria through elemental analysis, but elemental gold was not present in the spectrum (Fig. 3.6G, Fig. 3.6H), indicating that PEG-AuNPs did not bind to *A. baumannii*.

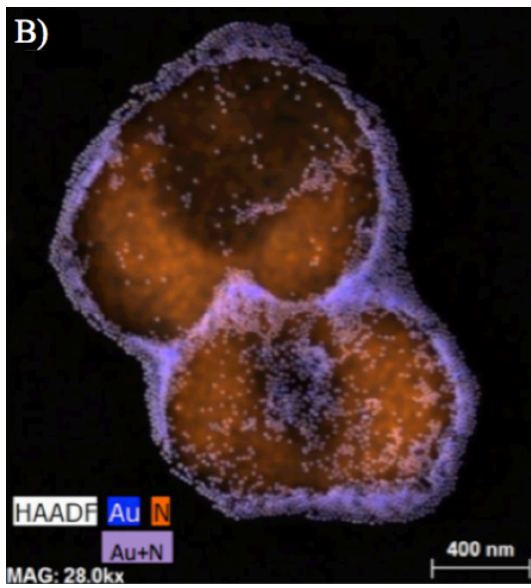
Col-PEG-AuNPs



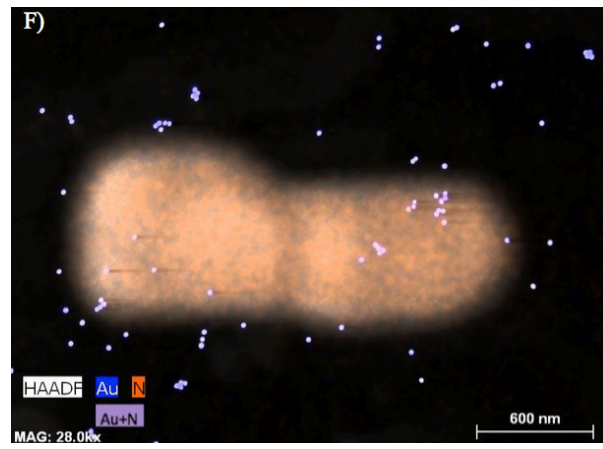
PEG-AuNPs



Col-PEG-AuNPs



PEG-AuNPs



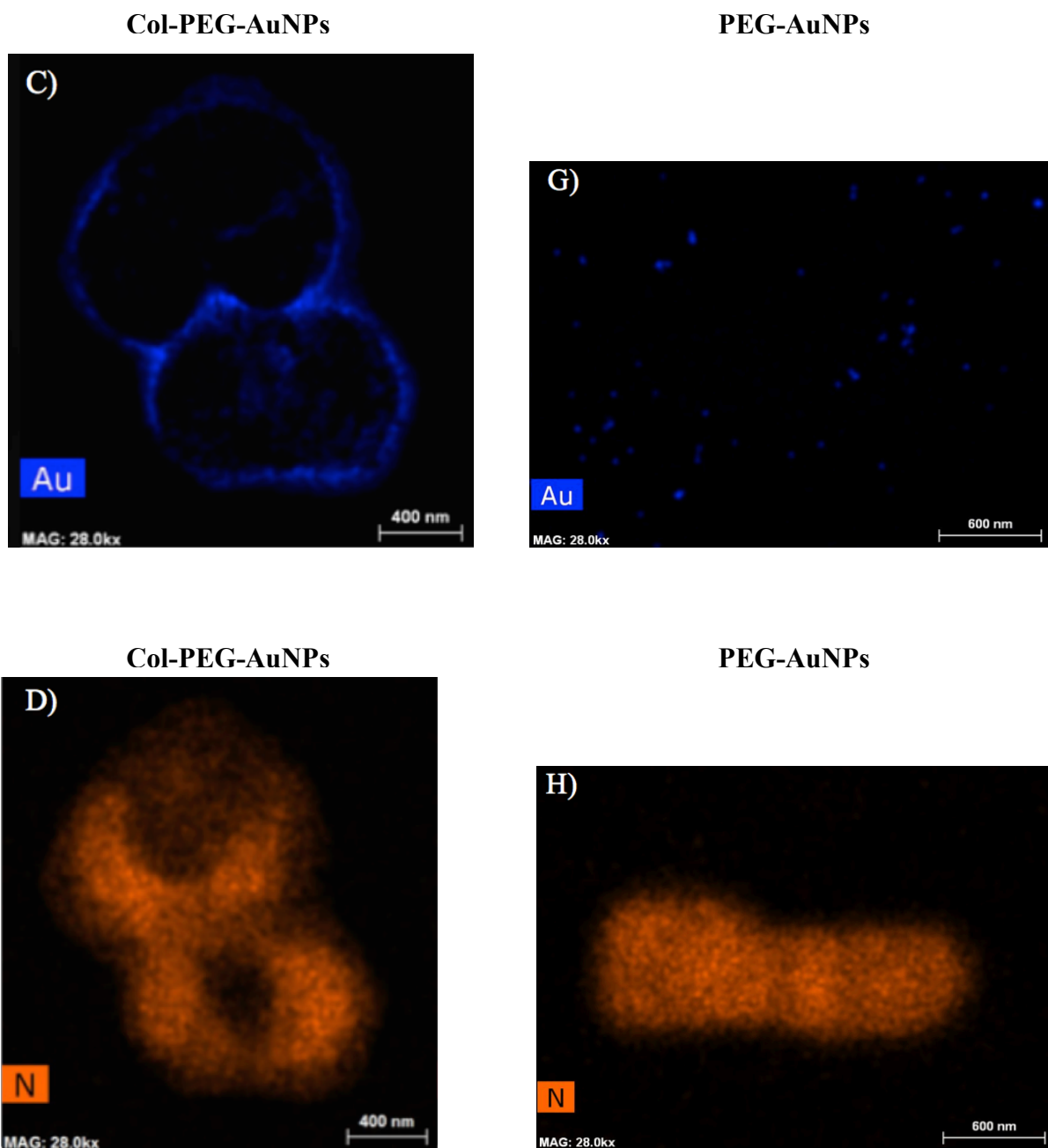


Figure 3.6. STEM imaging of (A) Col-PEG-AuNP association with *A. baumannii* suggests that the targeting ligand of colistin is required for nanoparticle binding to *A. baumannii*. A) STEM of Col-PEG-AuNPs bound to *A. baumannii*. B) HAADF-EDS view of the sample analyzed in panel (A). The sample was analyzed via HAADF imaging in combination with EDS for the presence of gold (C) and nitrogen (D). The EDS spectrum behind each pixel was used for elemental image analysis. E) STEM of PEG-AuNPs incubated with *A. baumannii*. F) HAADF-EDS view of the sample analyzed in panel (E). The sample was analyzed via EDS for the presence of gold (G) and nitrogen (H).

3.7. *A. baumannii* binding kinetics

Col-PEG-AuNP binding to *A. baumannii* was characterized as a function of the extent of colistin decoration per NP (Col:NP ratio), holding the NP:*A. baumannii* ratio constant. Fastest binding occurred when using a 15 μM colistin concentration functionalized to the AuNP surface, which is consistent with colistin concentrations administered in clinically approved treatments [71]. To achieve a 15 μM colistin concentration, approximately 3500 Colistin-PEG₃₄₀₀-OPSS ligands were bound to a single AuNP, based on the molecular dimensions of PEG, number of AuNPs, and volume of the AuNPs. The kinetics of Col-PEG-AuNP association with *A. baumannii* was characterized by a spin filtration technique as described in section 2.2.10. Following the addition of *A. baumannii* to Col-PEG-AuNPs, the rate of association was evaluated over a 2 h time period.

Nanoparticle attachment to *A. baumannii* was dependent upon the presence of the colistin targeting ligand, as shown in Figure 3.7. The rate of Col-PEG-AuNP binding to *A. baumannii* is described by a two-parameter, exponential curve in the form of:

$$A = A_{Max} * \left(1 - e^{-t/\tau}\right) \quad (1)$$

where A (number) represents the number of Col-PEG-AuNPs bound to a single *A. baumannii*, and t (min) represents time. The constants for the exponential curve are A_{Max} (maximum number of Col-PEG-AuNPs per *A. baumannii*), the final asymptotic value of this system, and τ (min), the time constant. The maximum number of Col-PEG-AuNPs bound to a single *A. baumannii* (A_{Max}) was estimated to be 1316 ± 182 . The time constant, τ , represents the time required for 63% of maximal Col-PEG-AuNP binding per *A. baumannii*, or A_{Max} . In this system, τ is equivalent to 10.7 ± 2.1 minutes. Therefore, Eq. (1) can be more completely represented as:

$$A = 1316 * \left(1 - e^{-t/10.7}\right) \quad (2)$$

Half-maximal binding occurs when A is equal to half of A_{Max} , or when 658 Col-PEG-AuNPs are bound to a single *A. baumannii*. Half-maximal binding occurred at 7.5 minutes. The PEG-AuNP control samples, in the absence of colistin, did not exhibit time dependent binding behavior (Fig. 3.7), further confirming colistin as necessary for PEG-AuNP association with *A. baumannii*.

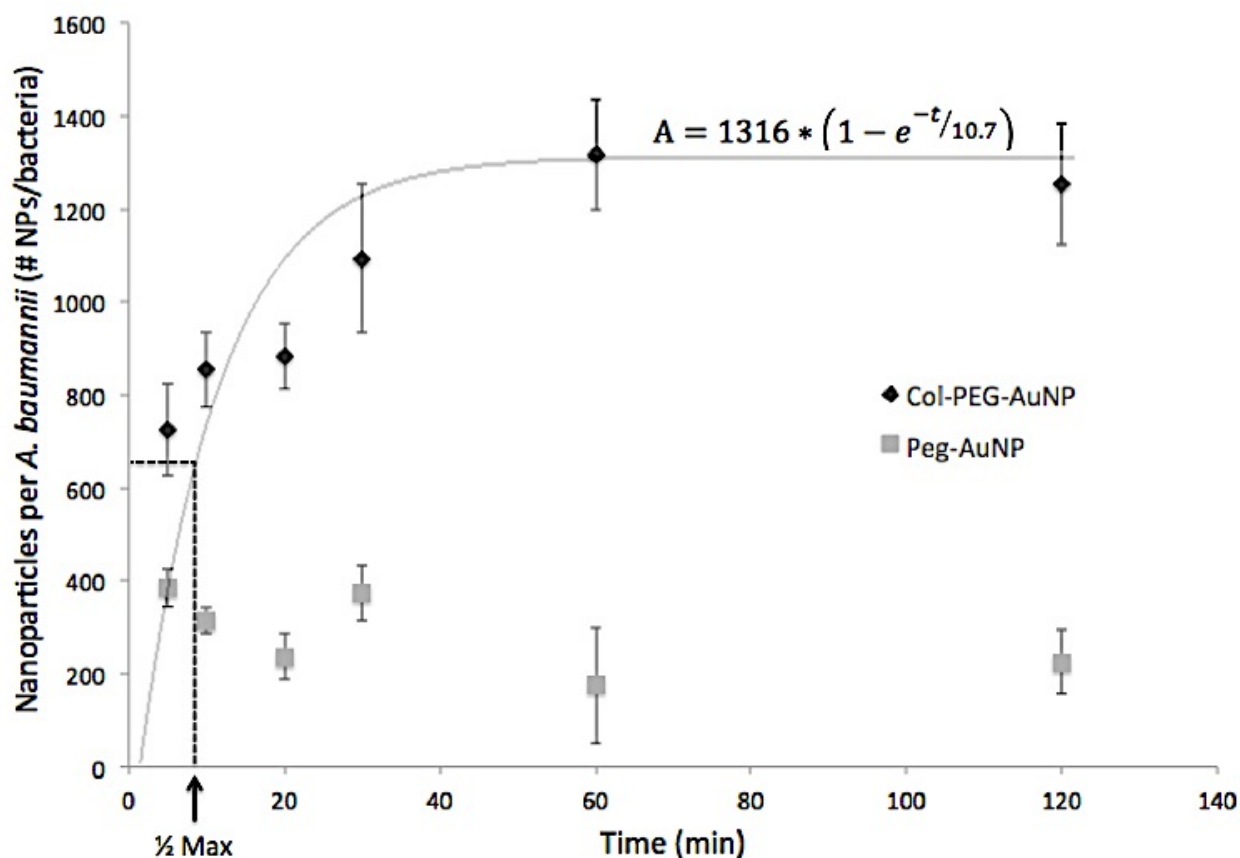


Figure 3.7. Col-PEG-AuNPs rapidly and specifically associated with *A. baumannii*, reaching 50% maximum saturation within 7.5 min, whereas PEG-AuNPs did not specifically bind the bacteria. Interaction of Col-PEG-AuNPs with *A. baumannii* was significantly different than the interaction of PEG-AuNPs with *A. baumannii*, as indicated at the 5 min time point. ANOVA and *post hoc* analysis prove that Col-PEG-AuNPs per *A. baumannii* at all time points are significantly different than those of PEG-AuNPs per *A. baumannii*.

CHAPTER 4

Summary

This work, for the first time, presented a mathematical description of the binding kinetics between colistin functionalized nanoparticles and *A. baumannii*. The novel nanoparticle system with colistin as an *A. baumannii* targeter covalently conjugated to the distal end of PEG eliminated the possibility of colistin disassembly through electrostatic interactions. Additionally, the use of a ligand reduced colistin steric hindrance and increased nanoparticle-bacteria association. On average, 658 colistin-functionalized nanoparticles associated with a single *A. baumannii* cell in approximately 7 min. This rapid rate of nanoparticle-bacteria association enables the consideration of new approaches to bacterial detection and isolation. Functionalizing magnetic core nanoparticles with Colistin-PEG₃₄₀₀-OPSS is projected to support magnetic extraction of particle-bound *A. baumannii* using methods similar to Singh et al. and Lee et al. [51], [58]. Because colistin is FDA approved and readily available, this design may be further developed and used in water treatment facilities to rid contaminated water of deadly pathogens, such as *A. baumannii*.

Nanoparticle bound Colistin-PEG₃₄₀₀-OPSS is biocompatible and can, therefore, be injected directly into the source of contaminated water for *in situ* treatment. Colistin-PEG₃₄₀₀-OPSS readily binds to its bacterial target, as indicated by Figure 3.7. Nanoparticles functionalized with Colistin-PEG₃₄₀₀-OPSS are an effective approach to water treatment because only small amounts are needed due to the significant ligand reactivity, as well as the large surface area of the nanoparticles. Their superiority to nanofiltration membranes, nanoporous

ceramics, nanofibers, and nanocatalysts lies in the fact that they offer a high surface area to volume ratio by being small and without introducing mass transfer limitations common to porous structures. Nanoparticles functionalized with Colistin-PEG₃₄₀₀-OPSS are versatile and can be applied to both treat effluents and sediment matrices. Also, the Colistin-PEG₃₄₀₀-OPSS ligand could potentially be bound to membranes for *ex situ* applications.

In the future, the use of colistin-functionalized nanoparticles for the rapid binding of *A. baumannii* may also enable new advances in the detection and purification of Gram-negative bacteria from other environmental samples, such as food and soil. *A. baumannii* proliferates over time, therefore, the detection of the bacterium in its early stages would be useful in preventing the transmission of infections. Also, the technology developed in this work could potentially be useful in the hospital setting where *A. baumannii* is known to cause a range of different infections, including the blood-borne infection sepsis. The Colistin-PEG₃₄₀₀-OPSS ligand developed in this work for the capture of *A. baumannii* has the potential to be used for the rapid selection of bacteria from blood. The binding kinetics seen between the Col-PEG-AuNPs and *A. baumannii* could allow for rapid NP-bacteria association in blood, thereby facilitating clinical applications with extracorporeal devices. Also, because colistin has been approved for use in the clinical setting for decades, the Colistin-PEG₃₄₀₀-OPSS ligand presents major advantages over other genetically engineered and biomacromolecular ligands used in this context.

Appendix:

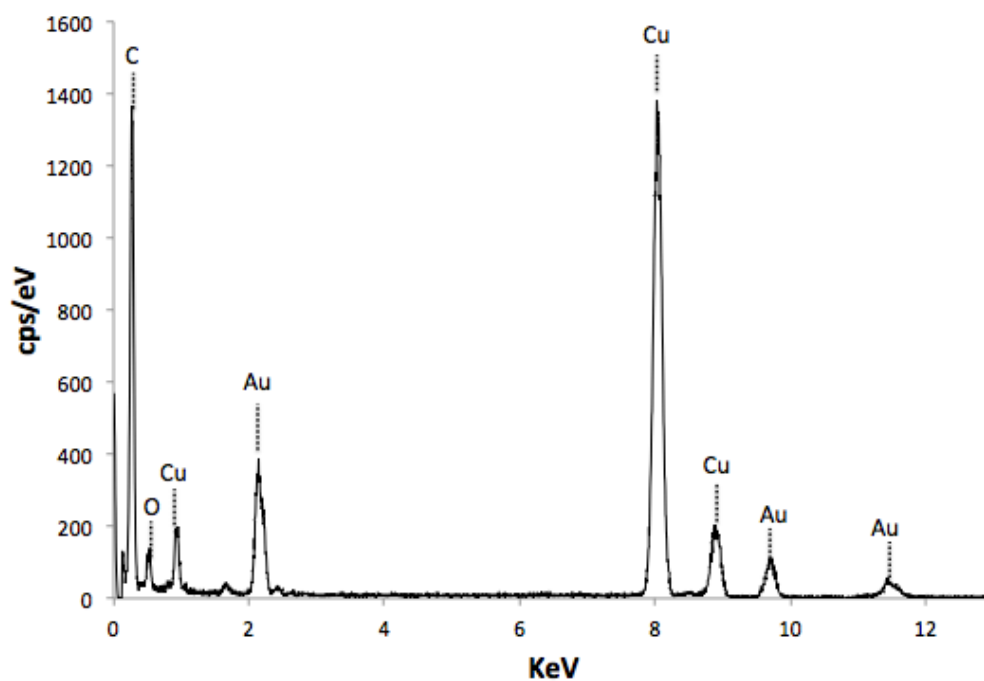


Figure S1. TEM-EDS of Col-PEG-AuNPs verified the presence of Au in the sample, confirming the nanoparticle core composition. The copper (Cu) signals were a result of the carbon film-backed copper grids used.

Table S1. Red Blood Cell Hemolysis	
Sample	Hemolysis (%)
0.25 mM Col-PEG-AuNPs	-0.3 ± 0.4
0.25 mM PEG-AuNPs	-2.7 ± 0.8
0.5 mM Col-PEG-AuNPs	1.2 ± 0.5
0.5 mM PEG-AuNPs	-0.4 ± 0.8
1.0 mM Col-PEG-AuNPs	-3.0 ± 0.2
1.0 mM PEG-AuNPs	-0.2 ± 0.7
2.0 mM Col-PEG-AuNPs	0.2 ± 0.4
2.0 mM PEG-AuNPs	-0.6 ± 0.8
Positive control (20% triton-X)	100 ± 1.9
Negative control (PBS, pH 7.4)	0.0 ± 0.0

Table S2. Red Blood Cell Hemolysis	
Sample	Hemolysis (%)
0.2 mM Free Colistin	-0.7 ± 0.6
0.4 mM Free Colistin	-0.8 ± 1.1
0.9 mM Free Colistin	0.8 ± 1.5
900 mM Free Colistin	-0.4 ± 0.8
Positive control (20% triton-X)	100 ± 1.9
Negative control (PBS, pH 7.4)	0.0 ± 0.0

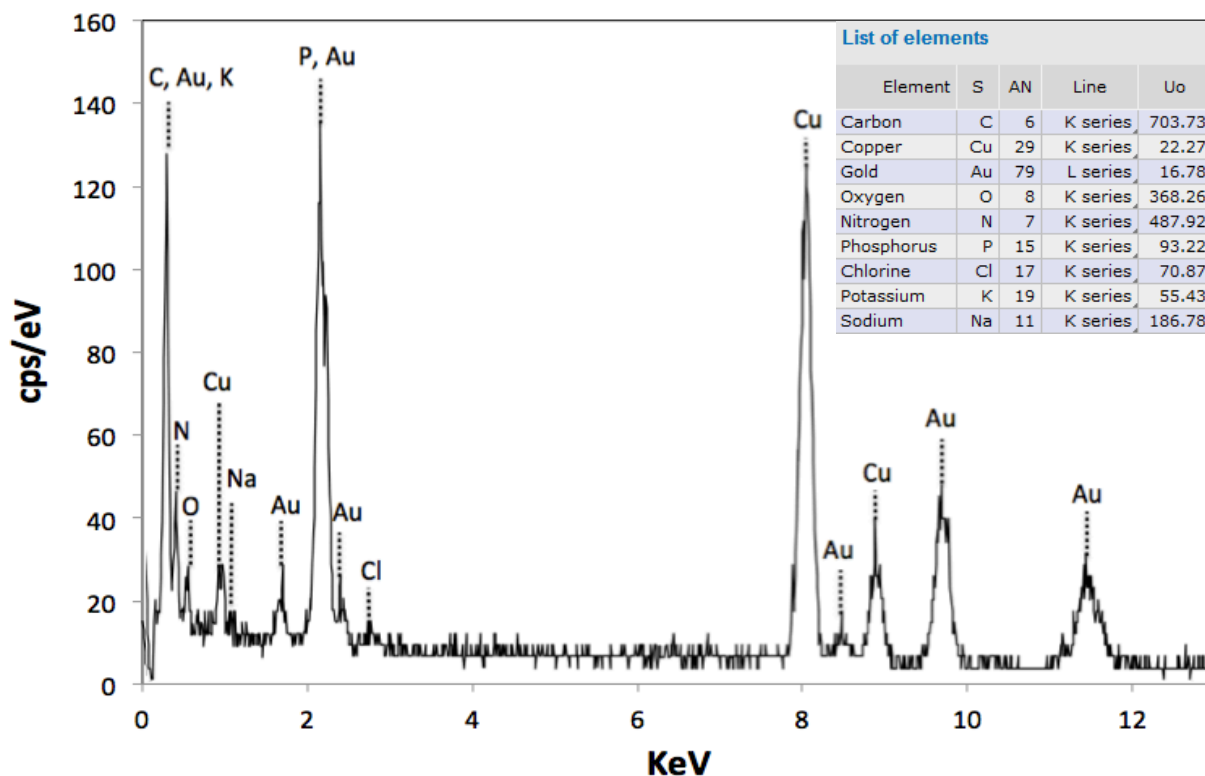


Figure S2. EDS spectrum of Fig. 3.6B confirmed that Col-PEG-AuNPs, indicated by Au peaks, were associated with *A. baumannii*, indicated by phosphate (P), potassium (K), sodium (Na), nitrogen (N), and chlorine (Cl) peaks. The Cu signals were a result of the carbon film-backed copper grids used.

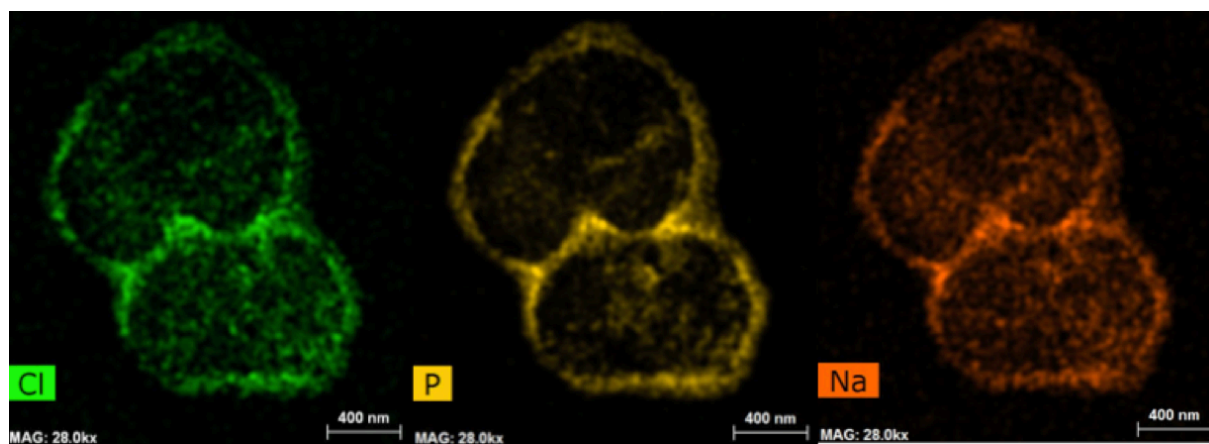
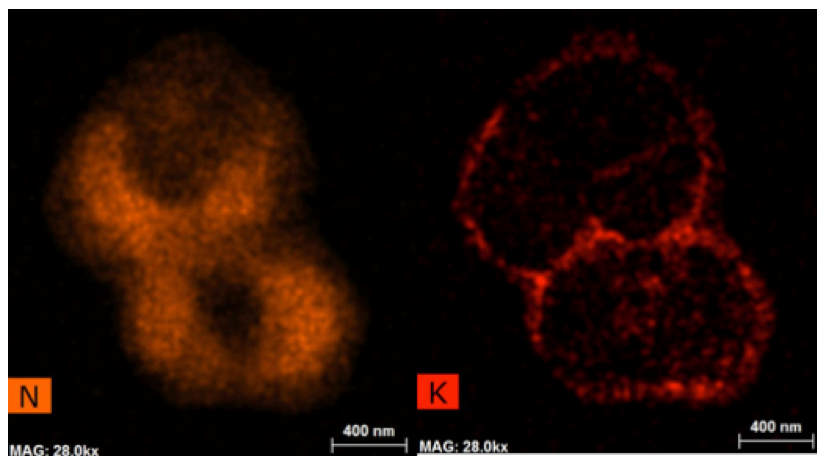


Figure S3. HAADF-STEM images in combination with EDS further confirmed the elemental composition of *A. baumannii*. N, K, Cl, P, and Na are the core elements that make up *A. baumannii*.

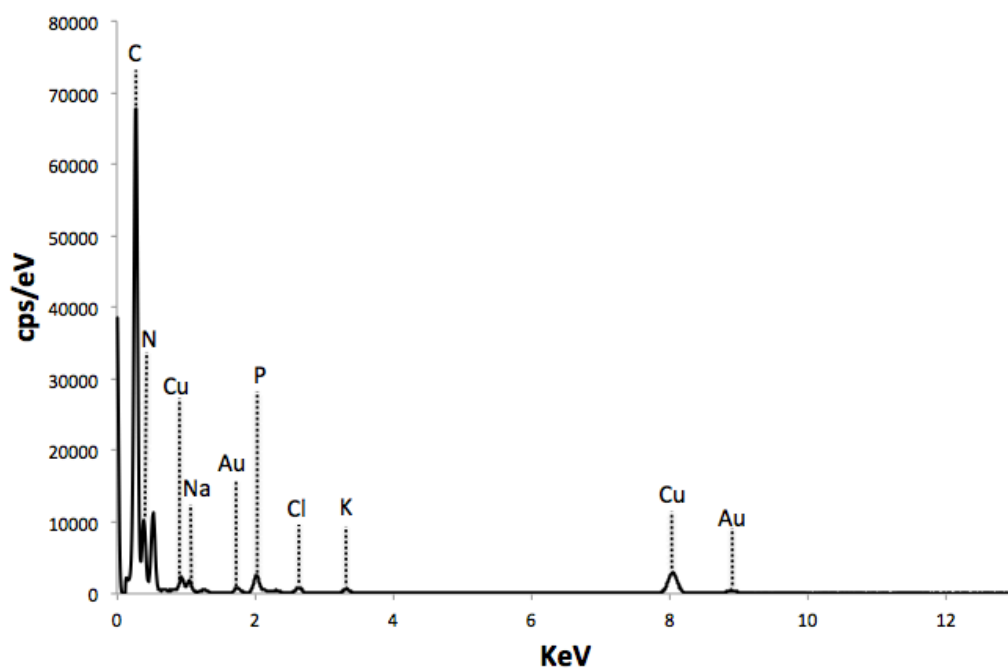


Figure S4. EDS spectrum of PEG-AuNPs incubated with *A. baumannii* lacks Au, indicating that PEG-AuNPs were not bound to *A. baumannii*. P, K, Na, and Cl peaks confirmed the presence of bacteria. The Cu signals were a result of the carbon film-backed copper grids used.

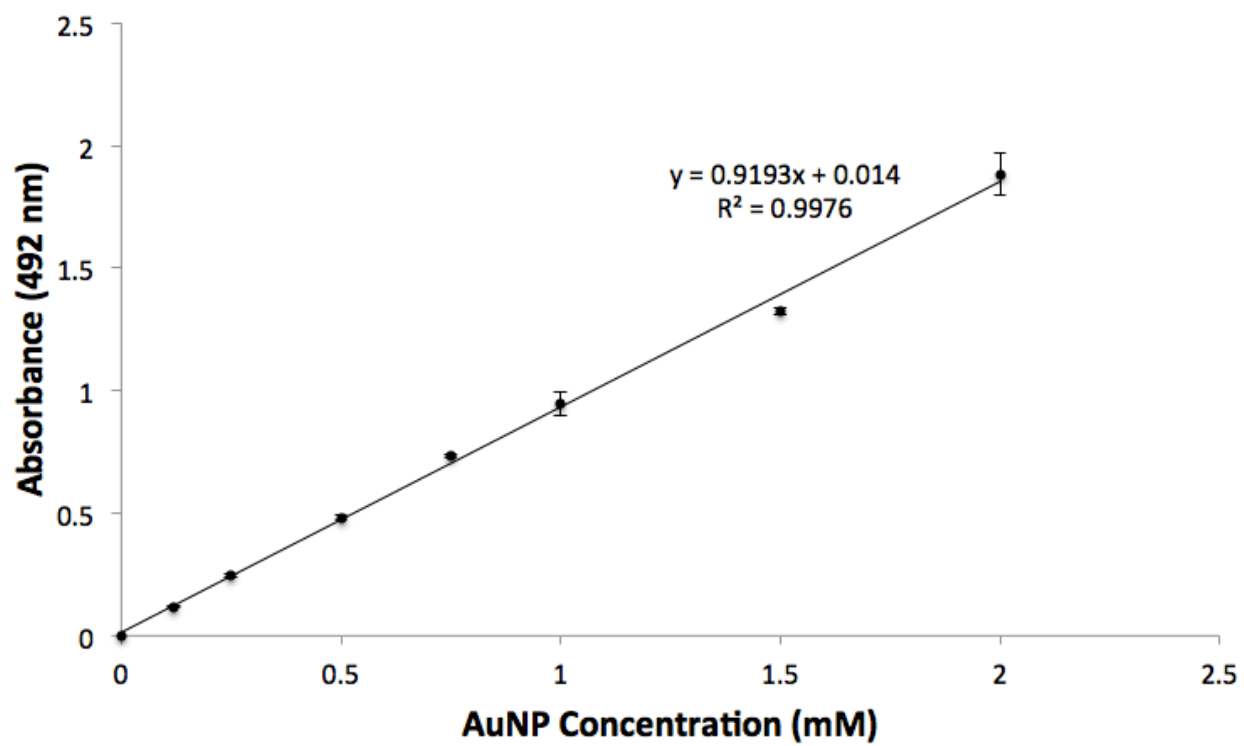


Figure S5. AuNP standard concentration curve based on absorbance.

REFERENCES

- [1] S. K. Nachimuthu and P. J. Haug, “Early Detection of Sepsis in the Emergency Department using Dynamic Bayesian Networks,” *AMIA Annu. Symp. Proc.*, vol. 2012, pp. 653–662, 2012.
- [2] P.-E. Fournier, D. Vallenet, V. Barbe, S. Audic, H. Ogata, L. Poirel, H. Richet, C. Robert, S. Mangenot, C. Abergel, P. Nordmann, J. Weissenbach, D. Raoult, and J.-M. Claverie, “Comparative genomics of multidrug resistance in *Acinetobacter baumannii*,” *PLoS Genet.*, vol. 2, no. 1, p. e7, Jan. 2006.
- [3] J.-L. Vincent, J. Rello, J. Marshall, E. Silva, A. Anzueto, C. D. Martin, R. Moreno, J. Lipman, C. Gomersall, Y. Sakr, and K. Reinhart, “International study of the prevalence and outcomes of infection in intensive care units,” *JAMA*, vol. 302, pp. 2323–2329, 2009.
- [4] L. L. Maragakis and T. M. Perl, “*Acinetobacter baumannii*: epidemiology, antimicrobial resistance, and treatment options,” *Clin. Infect. Dis.*, vol. 46, no. 8, pp. 1254–63, Apr. 2008.
- [5] H. J. Doughari, P. A. Ndakidemi, I. S. Human, and S. Benade, “The ecology, biology and pathogenesis of *Acinetobacter* spp.: an overview,” *Microbes Environ.*, vol. 26, no. 2, pp. 101–112, 2011.
- [6] “WHO | Guidelines for drinking-water quality, fourth edition 2011.”
- [7] E. J. Anaissie, S. R. Penzak, and M. C. Dignani, “The Hospital Water Supply as a Source of Nosocomial Infections,” *Arch. Intern. Med.*, vol. 162, no. 13, p. 1483, Jul. 2002.
- [8] K. Y. Nelson, D. W. McMartin, C. K. Yost, K. J. Runtz, and T. Ono, “Point-of-use water disinfection using UV light-emitting diodes to reduce bacterial contamination,” *Environ. Sci. Pollut. Res. Int.*, vol. 20, no. 8, pp. 5441–8, Aug. 2013.
- [9] N. J. Ashbolt, “Microbial contamination of drinking water and disease outcomes in developing regions,” *Toxicology*, vol. 198, no. 1–3, pp. 229–38, May 2004.
- [10] “WHO | Water supply, sanitation and hygiene development.”

- [11] U. Förstner and G. T. W. Wittmann, *Metal Pollution in the Aquatic Environment*. Springer Science & Business Media, 2012.
- [12] C. Zhang, S. Qiu, Y. Wang, L. Qi, R. Hao, X. Liu, Y. Shi, X. Hu, D. An, Z. Li, P. Li, L. Wang, J. Cui, P. Wang, L. Huang, J. D. Klena, and H. Song, “Higher isolation of NDM-1 producing *Acinetobacter baumannii* from the sewage of the hospitals in Beijing.,” *PLoS One*, vol. 8, no. 6, p. e64857, Jan. 2014.
- [13] N. Savage and M. S. Diallo, “Nanomaterials and water purification: Opportunities and challenges,” in *Journal of Nanoparticle Research*, 2005, vol. 7, no. 4–5, pp. 331–342.
- [14] I. Ali, “New generation adsorbents for water treatment,” *Chemical Reviews*, vol. 112, no. 10, pp. 5073–5091, 2012.
- [15] S. Singh, K. C. Barick, and D. Bahadur, “Surface engineered magnetic nanoparticles for removal of toxic metal ions and bacterial pathogens.,” *J. Hazard. Mater.*, vol. 192, no. 3, pp. 1539–47, 2011.
- [16] A. Itodo, F. Abdulrahman, L. Hassan, S. a. Maigandi, and H. Itodo, “Intraparticle diffusion and intraparticulate diffusivities of herbicide on derived activated carbon,” *Researcher*, vol. 2, no. 2, pp. 74–86, 2010.
- [17] T. Hillie and M. Hlophe, “Nanotechnology and the challenge of clean water.,” *Nat. Nanotechnol.*, vol. 2, no. 11, pp. 663–4, Nov. 2007.
- [18] J. Theron, J. a Walker, and T. E. Cloete, “Nanotechnology and water treatment: applications and emerging opportunities.,” *Crit. Rev. Microbiol.*, vol. 34, no. 1, pp. 43–69, 2008.
- [19] R. D. Ambashta and M. Sillanpää, “Water purification using magnetic assistance: a review.,” *J. Hazard. Mater.*, vol. 180, no. 1–3, pp. 38–49, Aug. 2010.
- [20] L. N. Rao, “Nanotechnological Methodology for Treatment of Waste water,” *Int. J. ChemTech Res.*, vol. 6, no. 4, p. 2529, 2014.
- [21] S. Kar, R. C. Bindal, and P. K. Tewari, “Carbon nanotube membranes for desalination and water purification: Challenges and opportunities,” *Nano Today*, vol. 7, no. 5, pp. 385–389, 2012.

- [22] B. Pan and B. Xing, "Adsorption Mechanisms of Organic Chemicals on Carbon Nanotubes," *Environ. Sci. Technol.*, vol. 42, no. 24, pp. 9005–9013, Dec. 2008.
- [23] C. Lu, Y.-L. Chung, and K.-F. Chang, "Adsorption of trihalomethanes from water with carbon nanotubes.," *Water Res.*, vol. 39, no. 6, pp. 1183–9, Mar. 2005.
- [24] R. Q. Long and R. T. Yang, "Carbon Nanotubes as Superior Sorbent for Dioxin Removal," *J. Am. Chem. Soc.*, vol. 123, no. 9, pp. 2058–2059, Mar. 2001.
- [25] V. K. K. Upadhyayula, S. Deng, M. C. Mitchell, and G. B. Smith, "Application of carbon nanotube technology for removal of contaminants in drinking water: a review.," *Sci. Total Environ.*, vol. 408, no. 1, pp. 1–13, Dec. 2009.
- [26] R. Andrews, D. Jacques, A. M. Rao, F. Derbyshire, D. Qian, X. Fan, E. C. Dickey, and J. Chen, "Continuous production of aligned carbon nanotubes: a step closer to commercial realization," *Chem. Phys. Lett.*, vol. 303, no. 5–6, pp. 467–474, Apr. 1999.
- [27] G. S. Simate, S. E. Iyuke, S. Ndlovu, M. Heydenrych, and L. F. Walubita, "Human health effects of residual carbon nanotubes and traditional water treatment chemicals in drinking water.," *Environ. Int.*, vol. 39, no. 1, pp. 38–49, Feb. 2012.
- [28] C.-W. Lam, J. T. James, R. McCluskey, S. Arepalli, and R. L. Hunter, "A review of carbon nanotube toxicity and assessment of potential occupational and environmental health risks.," *Crit. Rev. Toxicol.*, vol. 36, no. 3, pp. 189–217, 2006.
- [29] J. Kolosnjaj, H. Szwarc, and F. Moussa, "Toxicity Studies of Carbon Nanotubes," in *Bio-Applications of Nanoparticles*, vol. 620, 2007, pp. 181–204.
- [30] J. G. Moralez, J. Raez, T. Yamazaki, R. K. Motkuri, A. Kovalenko, and H. Fenniri, "Helical rosette nanotubes with tunable stability and hierarchy," *J. Am. Chem. Soc.*, vol. 127, no. 23, pp. 8307–8309, 2005.
- [31] R. S. Johnson, T. Yamazaki, A. Kovalenko, and H. Fenniri, "Molecular basis for water-promoted supramolecular chirality inversion in helical rosette nanotubes," *J. Am. Chem. Soc.*, vol. 129, pp. 5735–5743, 2007.
- [32] "Overview and Comparison of Conventional and Nano-Based Water Treatment Technologies," *Carbon N. Y.*, pp. 1–38, 2006.

- [33] R. Margesin and F. Schinner, "Biodegradation and bioremediation of hydrocarbons in extreme environments," *Appl. Microbiol. Biotechnol.*, vol. 56, no. 5–6, pp. 650–663, 2001.
- [34] N. Liu, L. Li, B. McPherson, and R. Lee, "Removal of organics from produced water by reverse osmosis using MFI-type zeolite membranes," *J. Memb. Sci.*, vol. 325, no. 1, pp. 357–361, 2008.
- [35] M. Kazemimoghadam, "New nanopore zeolite membranes for water treatment," *Desalination*, vol. 251, no. 1–3, pp. 176–180, 2010.
- [36] M. M. Pendergast and E. M. V. Hoek, "A review of water treatment membrane nanotechnologies," *Energy Environ. Sci.*, vol. 4, no. 6, p. 1946, Jun. 2011.
- [37] Z. MA, M. KOTAKI, and S. RAMAKRISHNA, "Electrospun cellulose nanofiber as affinity membrane," *J. Memb. Sci.*, vol. 265, no. 1–2, pp. 115–123, Nov. 2005.
- [38] H. Ma, C. Burger, B. S. Hsiao, and B. Chu, "Ultrafine polysaccharide nanofibrous membranes for water purification.," *Biomacromolecules*, vol. 12, no. 4, pp. 970–6, Apr. 2011.
- [39] R. BARHATE and S. RAMAKRISHNA, "Nanofibrous filtering media: Filtration problems and solutions from tiny materials," *J. Memb. Sci.*, vol. 296, no. 1–2, pp. 1–8, Jun. 2007.
- [40] S. Homaeigohar and M. Elbahri, "Nanocomposite Electrospun Nanofiber Membranes for Environmental Remediation," *Materials (Basel)*, vol. 7, no. 2, pp. 1017–1045, Feb. 2014.
- [41] T. J. Menkhaus, H. Varadaraju, L. Zhang, S. Schneiderman, S. Bjustrom, L. Liu, and H. Fong, "Electrospun nanofiber membranes surface functionalized with 3-dimensional nanolayers as an innovative adsorption medium with ultra-high capacity and throughput," *Chem. Commun.*, vol. 46, no. 21, p. 3720, May 2010.
- [42] H. Zhang, X. Quan, S. Chen, and H. Zhao, "Fabrication and characterization of silica/titania nanotubes composite membrane with photocatalytic capability," *Environ. Sci. Technol.*, vol. 40, no. 19, pp. 6104–6109, 2006.
- [43] X. Z. Li, H. Liu, L. F. Cheng, and H. J. Tong, "Photocatalytic oxidation using a new

- catalyst--TiO₂ microsphere--for water and wastewater treatment,” *Env. Sci Technol*, vol. 37, no. 17, pp. 3989–3994, 2003.
- [44] M. N. Chong, B. Jin, C. W. K. Chow, and C. Saint, “Recent developments in photocatalytic water treatment technology: A review,” *Water Research*, vol. 44, no. 10, pp. 2997–3027, 2010.
- [45] H. A. Foster, I. B. Ditta, S. Varghese, and A. Steele, “Photocatalytic disinfection using titanium dioxide: spectrum and mechanism of antimicrobial activity.,” *Appl. Microbiol. Biotechnol.*, vol. 90, no. 6, pp. 1847–68, Jun. 2011.
- [46] P. C. Maness, S. Smolinski, D. M. Blake, Z. Huang, E. J. Wolfrum, and W. A. Jacoby, “Bactericidal activity of photocatalytic TiO₂ reaction: toward an understanding of its killing mechanism.,” *Appl. Environ. Microbiol.*, vol. 65, no. 9, pp. 4094–8, Sep. 1999.
- [47] I. B. Ditta, A. Steele, C. Liptrot, J. Tobin, H. Tyler, H. M. Yates, D. W. Sheel, and H. A. Foster, “Photocatalytic antimicrobial activity of thin surface films of TiO₂, CuO and TiO₂/CuO dual layers on Escherichia coli and bacteriophage T4.,” *Appl. Microbiol. Biotechnol.*, vol. 79, no. 1, pp. 127–33, May 2008.
- [48] T. P. T. Cushnie, P. K. J. Robertson, S. Officer, P. M. Pollard, C. McCullagh, and J. M. C. Robertson, “Variables to be considered when assessing the photocatalytic destruction of bacterial pathogens.,” *Chemosphere*, vol. 74, no. 10, pp. 1374–8, Mar. 2009.
- [49] J.-W. Liou and H.-H. Chang, “Bactericidal effects and mechanisms of visible light-responsive titanium dioxide photocatalysts on pathogenic bacteria.,” *Arch. Immunol. Ther. Exp. (Warsz.)*, vol. 60, no. 4, pp. 267–75, Aug. 2012.
- [50] Y. F. Shen, J. Tang, Z. H. Nie, Y. D. Wang, Y. Ren, and L. Zuo, “Tailoring size and structural distortion of Fe₃O₄ nanoparticles for the purification of contaminated water.,” *Bioresour. Technol.*, vol. 100, no. 18, pp. 4139–46, 2009.
- [51] S. Singh, K. C. Barick, and D. Bahadur, “Surface engineered magnetic nanoparticles for removal of toxic metal ions and bacterial pathogens.,” *J. Hazard. Mater.*, vol. 192, no. 3, pp. 1539–47, Sep. 2011.
- [52] D. E. Kang, J. H. Super, M. Yung, C. W. Cooper, R. M. Domansky, K. Graveline, A. R., . . . Ingber, “An extracorporeal blood-cleansing device for sepsis therapy,” *Nat Med*, vol. 20, no. 10, pp. 1211–1216, 2014.

- [53] W. Yantasee, C. L. Warner, T. Sangvanich, R. S. Addleman, T. G. Carter, R. J. Wiacek, G. E. Fryxell, C. Timchalk, and M. G. Warner, "Removal of heavy metals from aqueous systems with thiol functionalized superparamagnetic nanoparticles.," *Environ. Sci. Technol.*, vol. 41, no. 14, pp. 5114–5119, 2007.
- [54] X. Liu, Q. Hu, Z. Fang, X. Zhang, and B. Zhang, "Magnetic chitosan nanocomposites: A useful recyclable tool for heavy metal ion removal," *Langmuir*, vol. 25, no. 1, pp. 3–8, 2009.
- [55] D. Decolin, P. Leroy, A. Nicolas, and P. Archimbault, "Hyphenated liquid chromatographic method for the determination of colistin residues in bovine tissues.," *J. Chromatogr. Sci.*, vol. 35, no. 12, pp. 557–564, 1997.
- [56] R. L. Soon, R. L. Nation, S. Cockram, J. H. Moffatt, M. Harper, B. Adler, J. D. Boyce, I. Larson, and J. Li, "Different surface charge of colistin-susceptible and -resistant *Acinetobacter baumannii* cells measured with zeta potential as a function of growth phase and colistin treatment.," *J. Antimicrob. Chemother.*, vol. 66, no. 1, pp. 126–33, Jan. 2011.
- [57] R. E. Hancock and D. S. Chapple, "Peptide antibiotics.," *Antimicrob. Agents Chemother.*, vol. 43, no. 6, pp. 1317–23, Jun. 1999.
- [58] J.-J. Lee, K. J. Jeong, M. Hashimoto, A. H. Kwon, A. Rwei, S. A. Shankarappa, J. H. Tsui, and D. S. Kohane, "Synthetic ligand-coated magnetic nanoparticles for microfluidic bacterial separation from blood.," *Nano Lett.*, vol. 14, no. 1, pp. 1–5, Jan. 2014.
- [59] J. H. Kang, M. Super, C. W. Yung, R. M. Cooper, K. Domansky, A. R. Graveline, T. Mammoto, J. B. Berthet, H. Tobin, M. J. Cartwright, A. L. Watters, M. Rottman, A. Waterhouse, A. Mammoto, N. Gamini, M. J. Rodas, A. Kole, A. Jiang, T. M. Valentin, A. Diaz, K. Takahashi, and D. E. Ingber, "An extracorporeal blood-cleansing device for sepsis therapy.," *Nat. Med.*, vol. 20, no. 10, pp. 1211–1216, Sep. 2014.
- [60] T. M. Phillips, *Encyclopedia of Chromatography, Volume 1*, 3rd ed. Taylor and Francis, 2005.
- [61] O. Uzun, Y. Hu, A. Verma, S. Chen, A. Centrone, and F. Stellacci, "Water-soluble amphiphilic gold nanoparticles with structured ligand shells.," *Chem. Commun. (Camb.)*, no. 2, pp. 196–8, Jan. 2008.
- [62] R. Hamid, Y. Rotshteyn, L. Rabadi, R. Parikh, and P. Bullock, "Comparison of alamar blue and MTT assays for high through-put screening," *Toxicol. Vitro.*, vol. 18, no. 5, pp.

703–710, 2004.

- [63] B. C. Evans, C. E. Nelson, S. S. Yu, K. R. Beavers, A. J. Kim, H. Li, H. M. Nelson, T. D. Giorgio, and C. L. Duvall, “Ex vivo red blood cell hemolysis assay for the evaluation of pH-responsive endosomolytic agents for cytosolic delivery of biomacromolecular drugs.,” *J. Vis. Exp.*, p. e50166, 2013.
- [64] C. Loo, A. Lowery, N. Halas, J. West, and R. Drezek, “Immunotargeted nanoshells for integrated cancer imaging and therapy,” *Nano Lett.*, vol. 5, pp. 709–711, 2005.
- [65] S. L. Sewell and T. D. Giorgio, “Synthesis and enzymatic cleavage of dual-ligand quantum dots,” *Mater. Sci. Eng. C*, vol. 29, pp. 1428–1432, 2009.
- [66] W. Brown, B. Iverson, E. Anslyn, and C. Foote, *Organic Chemistry*. Cengage Learning, 2013.
- [67] C. Carrillo-Carrión, B. M. Simonet, and M. Valcárcel, “Colistin-functionalised CdSe/ZnS quantum dots as fluorescent probe for the rapid detection of Escherichia coli.,” *Biosens. Bioelectron.*, vol. 26, no. 11, pp. 4368–74, Jul. 2011.
- [68] J. A. Orwa, C. Govaeris, R. Busson, E. Roets, A. VAN Schepdael, and J. Hoogmartens, “Isolation and Structural Characterization of Colistin Components.,” *J. Antibiot. (Tokyo)*, vol. 54, no. 7, pp. 595–599, Sep. 2001.
- [69] W. P. Wuelfing, S. M. Gross, D. T. Miles, and R. W. Murray, “Nanometer Gold Clusters Protected by Surface-Bound Monolayers of Thiolated Poly(ethylene glycol) Polymer Electrolyte,” *J. Am. Chem. Soc.*, vol. 120, no. 48, pp. 12696–12697, Dec. 1998.
- [70] S. N. Rampersad, “Multiple applications of Alamar Blue as an indicator of metabolic function and cellular health in cell viability bioassays.,” *Sensors (Basel)*, vol. 12, no. 9, pp. 12347–60, Jan. 2012.
- [71] M. E. Falagas and S. K. Kasiakou, “Colistin: the revival of polymyxins for the management of multidrug-resistant gram-negative bacterial infections.,” *Clin. Infect. Dis.*, vol. 40, no. 9, pp. 1333–1341, 2005.
- [72] H. Nose, G. W. Mack, X. R. Shi, and E. R. Nadel, “Shift in body fluid compartments after dehydration in humans.,” *J. Appl. Physiol.*, vol. 65, no. 1, pp. 318–24, Jul. 1988.

- [73] Q. He, J. Zhang, J. Shi, Z. Zhu, L. Zhang, W. Bu, L. Guo, and Y. Chen, "The effect of PEGylation of mesoporous silica nanoparticles on nonspecific binding of serum proteins and cellular responses," *Biomaterials*, vol. 31, no. 6, pp. 1085–1092, 2010.
- [74] Chan, S., S. R. Horner, A. Fauchet, P. M., and B. L. Miller, "Identification of Gram Negative Bacteria Using Nanoscale Silicon Microcavities." American Chemical Society, 01-Nov-2001.
- [75] S. K. Ward, J. A. Heintz, R. M. Albrecht, and A. M. Talaat, "Single-cell elemental analysis of bacteria: quantitative analysis of polyphosphates in *Mycobacterium tuberculosis*," *Front. Cell. Infect. Microbiol.*, vol. 2, p. 63, Jan. 2012.
- [76] M. A. Rouf, "Spectrochemical analysis of inorganic elements in bacteria," *J. Bacteriol.*, vol. 88, no. 6, pp. 1545–1549, Dec. 1964.